^{7}Be solar neutrino line: A reflection of the central temperature distribution of the Sun

John N. Bahcall
Institute for Advanced Study, Princeton, New Jersey 08540
(Received 17 September 1993)

A precise test of the theory of stellar evolution can be performed by measuring the average difference in energy between the neutrino line produced by ^{7}Be electron capture in the solar interior and the corresponding neutrino line produced in a terrestrial laboratory. This energy shift is calculated to be 1.29 keV (to an accuracy of a few percent) for the dominant ground-state to ground-state transition. The energy shift is approximately equal to the average temperature of the solar core, computed by integrating the temperature over the solar interior with a weighting factor equal to the locally produced ^{7}Be neutrino emission. Therefore, a measurement of the energy shift is a measurement of the central temperature distribution of the Sun. The energy profile of the ^{7}Be line is derived analytically and is evaluated numerically. The line shape is asymmetric: on the low-energy side, the line shape is Gaussian with a half-width at half-maximum of 0.6 keV and, on the high-energy side, the line shape is exponential with a half-width at half-maximum of 1.1 keV. The effective temperature of the high-energy exponential tail is 15×10^6 K. The energy profile of the ^{7}Be neutrino line should be taken into account in calculations of vacuum neutrino oscillations and of the absorption cross section for ^{7}Be solar neutrinos incident on ^{7}Li nuclei. The characteristic modulation of the ^{7}Be line shape that would be caused by either vacuum neutrino oscillations or by matter-enhanced (MSW) neutrino oscillations is shown to be small. Other frequently discussed weak interaction solutions to the solar neutrino problem are also not expected to change significantly the line profile.

PACS number(s): 96.60.Kx, 12.15.Ff, 14.60.Pq

I. INTRODUCTION

A. Background

The original motivation [1] for performing solar neutrino experiments was to learn more about how the Sun shines. When the first observational results from the chlorine experiment became available [2], the focus shifted [3] from learning about the interior of the Sun to trying to determine if the discrepancy between calculation and observation was due to inadequacies in the astrophysics or to new weak interaction physics. Directed toward this goal, four experiments are being performed [4–7] to measure the fluxes of neutrinos that are produced by nuclear fusion reactions in the solar interior. An additional four solar neutrino experiments [8–11], designed to determine if new physics or new astronomy is required, are being developed.

Progress toward the goal of testing solar theory by measuring solar neutrinos has been complicated by what may be the discovery of new weak interaction physics. A comparison of two of the existing experiments, the chlorine [4] and the Kamiokande [5] experiments, suggests [12] the existence of a physical process that changes, in a way that depends upon neutrino energy, the fraction of electron-type neutrinos that reach detectors on Earth after being created in the core of the Sun.

At first glance, the terrestrially observed flux of ^{8}B neutrinos is encouragingly close to the flux calculated on the basis of the standard solar model and the standard electroweak theory, especially considering the sensitivity of the predicted flux to details of the stellar physics. However, the discrepancy between calculation and observation is significant since the theoretical uncertainties are smaller than the difference between what is measured and what is predicted [13–15]. This discrepancy has stimulated a number of imaginative and attractive possible interpretations in terms of new physical processes [16–22]. Until the effects of these proposed new physical processes are either established or rejected experimentally, quantitative astronomical inferences from the measured magnitudes of the solar neutrino fluxes will be limited.

B. The ^{7}Be energy profile

The purpose of this paper is to draw attention to precise new predictions of the theory of stellar evolution that can be tested with the aid of future solar neutrino experiments. These new predictions are based upon the calculated shape of the energy spectrum of neutrinos produced by ^{7}Be electron capture in the solar interior. The reaction in question is

$$e^- + {}^7\mathrm{Be} \rightarrow {}^7\mathrm{Li} + \nu_e \,. \tag{1}$$

In the interior of the Sun, most of the electrons are captured from continuum (unbound) states [23,24]. The electron-capture reaction shown in (1) produces a neutrino line because the ^{7}Li nucleus in the final state has

a mass that is much greater than the energy of the neutrino. The recoiling nucleus takes up a significant amount of momentum, but only a negligible amount of energy. The focus of this paper is on the broadening by thermal effects of the neutrino line produced in the Sun.

This paper shows that the line shape for Eq. (1) reflects accurately the temperature distribution in the interior of the Sun. As we shall see, the difference between the average energy of the neutrino line emitted in the Sun and in the laboratory is approximately equal to the central temperature of the Sun (see especially Secs. V B and VI B). The predicted 1.3 keV increase in the average energy of the solar ^{7}Be neutrino line relative to laboratory decays is the simplest quantity to measure that directly reflects the solar temperature distribution.

In addition to a shift in the average neutrino energy, the shape of the line profile for ^{7}Be electron capture in the Sun is different from the line profile that would be observed for a laboratory source of ^{7}Be neutrinos. The shift in average energy and the change in the shape of the line profile are both caused by the high temperatures in the core of the Sun where the neutrinos are produced. The high solar temperatures produce significant thermal energies for continuum electrons and their capturing nuclei, Doppler shifts of the emitting nuclei, a high degree of ionization of solar ^{7}Be ions, and a difference in atomic binding energies for solar and laboratory ^{7}Be atoms.[1]

Figure 1 shows the two nuclear transitions that occur when ^{7}Be captures an electron in the laboratory. The neutrino energy corresponding to the transition from the ground state of ^{7}Be to the ground state of ^{7}Li will be denoted by $q_{\rm lab}$(g.s.); the energy corresponding to the transition to the first excited state of ^{7}Li will be denoted by $q_{\rm lab}$(e.s.). In what follows, I will discuss both transitions on an equal basis since the physical processes determining the neutrino line shape are the same in both cases. However, the transition to the ground state of ^{7}Li is more easily studied experimentally because it has a higher energy and a larger branching ratio [27]. Both the higher energy and the larger branching ratio of the ground-state to ground-state transition contribute to making the expected rate for this transition faster by an order of magnitude than for the ground-state to excited-state transition.

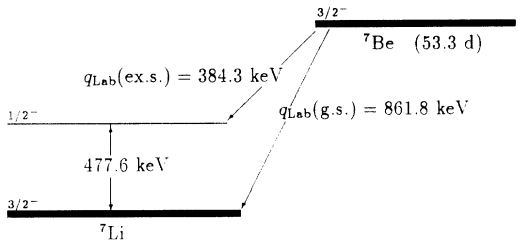

FIG. 1. The ^{7}Be decay scheme. The laboratory decay scheme for ^{7}Be is shown. The neutrino energies emitted in the ground-state to ground-state decay (branching ratio: 89.7%) and in the ground-state to excited-state decay (branching ratio 10.3%) are denoted, respectively, by $q_{\rm lab}$(g.s.) and $q_{\rm lab}$(e.s.). Details of the nuclear physics properties are summarized in [27].

For convenience, I will refer to the ground-state to ground-state transition as "ground-state" capture and will refer to the ground-state to excited-state transition as "excited-state" capture. In an additional effort to avoid cumbersome phrasing, I will often refer in the singular to "the" line profile or to "the" energy shift, when I mean the line profile or the energy shift for both ground-state capture and excited-state capture.

Before proceeding to the calculations, it is helpful to think about the following question. Why is the effect of the solar environment on the shape of the energy spectra for continuum β decays (one particle in the initial state, three particles in the final state, e.g., ^{8}B decay) different from the effect of solar conditions on the profile shape for the two-body electron capture reactions? This question has a simple physical answer.

If the simplest version of the standard electroweak model is correct, then the shape of the energy spectrum for electron-type neutrinos from continuum β decays in the Sun, such as the ^{8}B β decay, is independent of the conditions in the Sun to an accuracy of 1 part in 10^5 [28]. The invariance is a result of the fact that, in the center-of-momentum frame, a decaying ^{8}B nucleus has no kinetic energy. In the laboratory frame, terms of order the velocity of the nucleus, $v(^8\mathrm{B})/c$, cancel out because there are as many ^{8}B nuclei moving toward the observer as there are moving away from the observer. The first-order Doppler effects vanish because at each point within the broad ^{8}B continuum the neutrino energy is spread out symmetrically by a small amount. The largest potentially observable effects of the solar temperature on the observed ^{8}B neutrino energy spectrum are only second-order terms,$\sim v(^8\mathrm{B})^2/c^2$ [28]. This implication of standard theory will be tested by experiments [8,9,11] that will measure the shape of the ^{8}B neutrino energy spectrum and will compare the observed shape with the spectrum determined from terrestrial measurements.

By contrast, in the two-body electron-capture reactions, the profile of a narrow neutrino emission line is broadened asymmetrically by the solar temperature. On the low-energy side of the neutrino line profile, the dominant effect is first-order Doppler (or Gaussian) broadening caused by the motion of the decaying nuclei. On the high-energy side of the observed profile, the dominant effect is an exponential broadening resulting from the center-of-momentum kinetic energy of the electron and the decaying nucleus (for a physical discussion of the profile shape see especially Sec. VI). This asymmetric broadening causes a shift of the average energy of the neutrino line as well as change in the shape of the line profile.

[1] After the initial version of the present work was accepted for publication [25], my attention was directed by J. Pantaleone to two important papers [26]. In these two papers, the effect of the line width of the ^{7}Be and the $p + e^- + p$ (pep) lines on neutrino oscillations was calculated.

C. Experimental possibilities

A number of experiments [10,29] have been proposed that would measure predominantly the ν_e flux from ^{7}Be electron capture in the Sun, using detectors that are based upon neutrino-electron scattering. At the present time, the BOREXINO experiment [10] is the most advanced of these proposals and can, if recent estimates of the expected backgrounds are correct, measure the flux of ^{7}Be neutrinos. Radiochemical detectors of the flux of ^{7}Be neutrinos have also been discussed [30], but these detectors do not give specific information on neutrino energies. The radiochemical detectors are efficient for measuring the total flux of electron-type neutrinos above a specified energy threshold, but are not useful for studying the thermal effects investigated in this paper. Most recently, the use of a high resolution LiF bolometric detector of ^{7}Be neutrinos has been discussed [31].

Detectors have been developed [32] for a variety of other applications, including dark matter searches, the observation of double β decay, and x-ray astronomy, that have the energy resolution and the sensitivity that are required to study the energy spectrum of the ^{7}Be neutrino line. The best-available detectors have energy resolutions $\Delta E/E$ of much better than 1%, but they are smaller than would be required for a full-scale solar neutrino detector.

The most direct way to study the ^{7}Be energy profile may be to detect neutrino absorption by nuclei, a process which leaves an electron and a recoiling nucleus in the final state. In these charged-current transitions, nearly all of the initial neutrino energy is transferred to the final-state electron (the nuclear recoil energy being small). In the neutrino-electron scattering experiments that are currently under development, the 1 keV width of the ^{7}Be line is spread out over several hundred keV of electron recoil energy, since the neutrino and the electron share the final-state energy (see Fig. 8.5 of [13]).

In order to measure the predicted 1.3 keV (0.15%) energy shift via neutrino absorption, an energy resolution of order 1% to 0.1% is desirable, depending somewhat upon the absorption threshold. Consider, for specificity, a conceivable cryogenic experiment [33] that might be performed on ^{81}Br with an energy resolution of 1% and with a total of 10^3 measured neutrino events. The energy released to the recoil electron would be about 400 keV (the reaction threshold is about 450 keV), so the av-

TABLE I. The energy profile of the 862.0 keV ^{7}Be solar neutrino line. The neutrino energy is measured relative to the energy of the peak, which occurs at $q_{\rm peak} = 862.27$ keV. Here $P(q_{\rm obs} - q_{\rm peak}) = {\rm spectrum}_{\rm solar}(q_{\rm obs})$ is the probability that a neutrino of energy $q_{\rm obs}$ will be emitted between $q \pm 0.1$ keV.

$q_{\rm obs} - q_{\rm peak}$	$P(q_{\rm obs} - q_{\rm peak})$	$q_{\rm obs} - q_{\rm peak}$	$P(q_{\rm obs} - q_{\rm peak})$	$q_{\rm obs} - q_{\rm peak}$	$P(q_{\rm obs} - q_{\rm peak})$
−2.100	0.00000	1.000	0.26096	4.100	0.02526
−2.000	0.00000	1.100	0.24204	4.200	0.02341
−1.900	0.00001	1.200	0.22456	4.300	0.02169
−1.800	0.00004	1.300	0.20838	4.400	0.02010
−1.700	0.00012	1.400	0.19339	4.500	0.01863
−1.600	0.00032	1.500	0.17946	4.600	0.01726
−1.500	0.00082	1.600	0.16655	4.700	0.01600
−1.400	0.00197	1.700	0.15455	4.800	0.01482
−1.300	0.00442	1.800	0.14342	4.900	0.01373
−1.200	0.00928	1.900	0.13308	5.000	0.01272
−1.100	0.01825	2.000	0.12347	5.100	0.01179
−1.000	0.03359	2.100	0.11455	5.200	0.01092
−0.900	0.05787	2.200	0.10627	5.300	0.01012
−0.800	0.09338	2.300	0.09858	5.400	0.00937
−0.700	0.14115	2.400	0.09145	5.500	0.00868
−0.600	0.20014	2.500	0.08482	5.600	0.00805
−0.500	0.26666	2.600	0.07867	5.700	0.00745
−0.400	0.33448	2.700	0.07295	5.800	0.00690
−0.300	0.39629	2.800	0.06765	5.900	0.00640
−0.200	0.44517	2.900	0.06274	6.000	0.00592
−0.100	0.47662	3.000	0.05817	6.100	0.00549
0.000	0.48933	3.100	0.05394	6.200	0.00508
0.100	0.48515	3.200	0.05001	6.300	0.00471
0.200	0.46807	3.300	0.04636	6.400	0.00436
0.300	0.44285	3.400	0.04298	6.500	0.00404
0.400	0.41375	3.500	0.03984	6.600	0.00374
0.500	0.38390	3.600	0.03693	6.700	0.00347
0.600	0.35519	3.700	0.03423	6.800	0.00321
0.700	0.32846	3.800	0.03173	6.900	0.00297
0.800	0.30396	3.900	0.02941	7.000	0.00275
0.900	0.28153	4.000	0.02726		

erage neutrino energy would be measured to an accuracy of about 0.1 keV. The experimental parameters assumed in the above discussion would permit one to measure the central temperature of the sun to an accuracy of about 10%. In addition, a proposed high-pressure helium gas detector [34] might well have sufficient energy resolution to measure the predicted energy shift.

The requirements for a practical experiment may be achievable since the solar neutrino detectors currently under development are designed to detect several thousand events per year (albeit with much poorer energy resolution, typically $\sim 10\%$). It would be valuable to calibrate the solar results by studying an intense laboratory source of ^{7}Be neutrinos with the same detector as used in the solar observations. The work described in this paper was undertaken in the hope that it would stimulate an experiment that would measure the energy shift and perhaps other characteristics of the ^{7}Be line profile, in somewhat the same way that the initial theory and the experimental results on solar neutrinos developed together [1].

D. Organization and previous work

This paper is organized as described below. Section II presents calculations of the average neutrino energy release in the rest frame of the decaying particle when a ^{7}Be nucleus captures an electron under laboratory conditions (see Sec. II A) and in a solar environment (in which most of the electrons are captured from continuum orbits, see Sec. II B). Section III describes the central calculation of this paper, an evaluation of the energy profile for the neutrino line emitted when ^{7}Be nuclei capture continuum electrons that have a specified temperature. The following section, Sec. IV, outlines the calculation of the energy profile for the small but significant fraction of the solar electron captures that occur from bound orbits. The numerical characteristics of the line shape, including the shift in average neutrino energy between laboratory and solar decays, the full-width at half-maximum of the line profile, and the lower-order moments of the energy distribution, are the subject of Sec. V. The line profile is averaged, in this section, over the physical characteristics, including the temperature distribution, of detailed solar models. The numerical results are presented in Tables I and II and displayed in Figs. 2 and 3. Section VI provides approximate analytic derivations of the low-energy half-width (0.56 keV) and the high-energy half-width (1.07 keV) of the neutrino energy profile and isolates the separate physical origins of these two features. This section also presents a derivation of the shift in average neutrino energy between solar and laboratory decays

TABLE II. The energy profile of the 384.5 keV ^{7}Be solar neutrino line. The neutrino energy is measured relative to the energy of the peak which occurs at $q_{\rm peak} = 384.47$ keV. Here $P(q_{\rm obs} - q_{\rm peak}) = {\rm spectrum}_{\rm solar}(q_{\rm obs})$ is the probability that a neutrino of energy $q_{\rm obs}$ will be emitted between $q \pm 0.1$ keV.

$q_{\rm obs} - q_{\rm peak}$	$P(q_{\rm obs} - q_{\rm peak})$	$q_{\rm obs} - q_{\rm peak}$	$P(q_{\rm obs} - q_{\rm peak})$	$q_{\rm obs} - q_{\rm peak}$	$P(q_{\rm obs} - q_{\rm peak})$
−1.000	0.00000	1.800	0.16166	4.600	0.01956
−0.900	0.00000	1.900	0.15004	4.700	0.01812
−0.800	0.00002	2.000	0.13924	4.800	0.01679
−0.700	0.00022	2.100	0.12921	4.900	0.01556
−0.600	0.00187	2.200	0.11989	5.000	0.01442
−0.500	0.01152	2.300	0.11124	5.100	0.01336
−0.400	0.05065	2.400	0.10320	5.200	0.01238
−0.300	0.15855	2.500	0.09574	5.300	0.01147
−0.200	0.35442	2.600	0.08881	5.400	0.01063
−0.100	0.57417	2.700	0.08238	5.500	0.00985
0.000	0.69841	2.800	0.07641	5.600	0.00913
0.100	0.68431	2.900	0.07087	5.700	0.00846
0.200	0.60023	3.000	0.06573	5.800	0.00783
0.300	0.52127	3.100	0.06095	5.900	0.00726
0.400	0.46715	3.200	0.05652	6.000	0.00673
0.500	0.42841	3.300	0.05241	6.100	0.00623
0.600	0.39618	3.400	0.04859	6.200	0.00577
0.700	0.36720	3.500	0.04505	6.300	0.00535
0.800	0.34060	3.600	0.04177	6.400	0.00495
0.900	0.31603	3.700	0.03872	6.500	0.00459
1.000	0.29330	3.800	0.03590	6.600	0.00425
1.100	0.27224	3.900	0.03328	6.700	0.00394
1.200	0.25271	4.000	0.03085	6.800	0.00365
1.300	0.23460	4.100	0.02859	6.900	0.00338
1.400	0.21778	4.200	0.02650	7.000	0.00313
1.500	0.20216	4.300	0.02457	7.100	0.00290
1.600	0.18765	4.400	0.02277	7.200	0.00269
1.700	0.17418	4.500	0.02110		

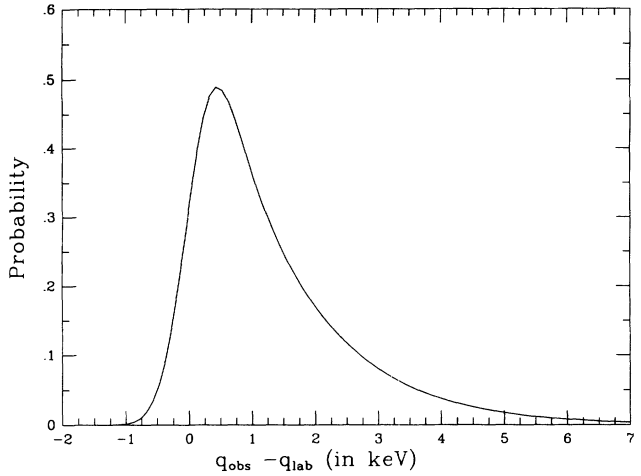

FIG. 2. The energy profile for the 862 keV line. The probability for the emission of a neutrino with energy q_{obs} in the laboratory frame is shown as a function of $q_{obs} - q_{lab}$, where the peak in the probability distribution is $q_{peak} = 862.27$ keV, 0.43 keV larger than the laboratory decay energy, $q_{lab} = 861.84$ keV. The probability distribution was computed by averaging Eqs. (46), (48), (49), (50), (56), and (57) over the Bahcall-Pinsonneault standard solar model with helium diffusion.

that explains why the shift is the same for ground-state and for excited-state captures. Section VII evaluates the effects on the neutrino line profile of electrostatic screening, of gravitational redshifts, and of collisional broadening, and shows that these effects are small. The influence of possible new weak interaction physics, exemplified by vacuum oscillations and by the MSW effect, is the subject of Sec. VIII. Neither type of oscillation would affect significantly the measurable characteristics of the ^{7}Be line profile. The energy shift and the asymmetric profile of the ^{7}Be line do change the computed absorption cross section for ^{7}Be solar neutrinos incident on a ^{7}Li detector, as is shown in Sec. IX. Section X summarizes the principal results of this paper.

There have been a number of previous calculations of the total rate for ^{7}Be electron capture in the Sun over the past three decades [23,24,35–39]. The present work on the ^{7}Be line shape does not change the results of these prior calculations of the total capture rate, the standard value in general use still being the one given in Ref. [35]. The only earlier work on the broadening of the ^{7}Be neutrino line with which I am familiar concentrated either on the fraction of electron-capture neutrinos that were above threshold for the $\nu_e + {}^7\mathrm{Li} \rightarrow {}^7\mathrm{Be} + e$ reaction, taking account of center-of-momentum energies but not Doppler shifts [37,38], or on a crude estimate of the total width, based only on the Doppler shifts of the ^{7}Be ions [13].

II. LABORATORY AND SOLAR ENERGIES

The average neutrino energy that is released when ^{7}Be captures an electron in a terrestrial laboratory is different from the average energy that is released when ^{7}Be captures an electron in the core of the Sun. In a laboratory experiment, all of the captured electrons are initially bound in a ^{7}Be atom, whereas in the solar interior most of the electron captures occur from continuum orbits [23]. Part of the difference in the average neutrino energy release, the part on which this section concentrates, is due, therefore, to the different atomic binding energies in the laboratory and in the Sun.

Energy conservation implies, for electron captures either in the Sun or in the laboratory, that

$$E_{\mathrm{initial}} - E_{\mathrm{final}} = \Delta M + K(e) + K(^7\mathrm{Be}) - K(^7\mathrm{Li}) - q + a(^7\mathrm{Be}) - a(^7\mathrm{Li}) = 0, \quad (2)$$

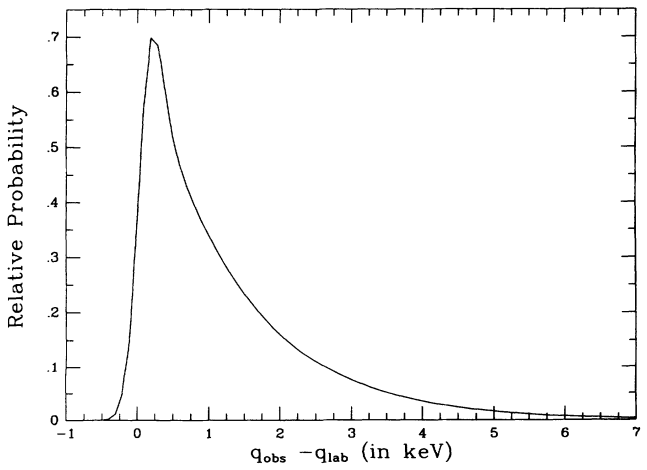

FIG. 3. The energy profile for the 384 keV line. This figure was computed in the same way as Fig. 2. The peak of this distribution lies at $q_{peak} = 384.47$ keV, 0.19 keV larger than the laboratory decay energy, $q_{lab} = 384.28$ keV.

where E_{initial} and E_{final} are the total energies in the initial and final states, $K(e)$ and $K(^7\mathrm{Be})$ are kinetic energies of the electron and of the ^{7}Be nucleus in the initial state, $K(^7\mathrm{Li})$ is the kinetic energy of the recoiling ^{7}Li nucleus, q is the neutrino energy, and $a(^7\mathrm{Be})$ and $a(^7\mathrm{Li})$ are the atomic binding energies. The quantity ΔM in Eq. (2) is the difference in rest mass energies [27], excluding atomic binding energies:

$$\Delta M = m_e + M(^7\mathrm{Be}) - M(^7\mathrm{Li}) = 862.10 \text{ keV}. \quad (3)$$

For electron captures that occur in the laboratory, the initial kinetic energies $K(e)$ and $K(^7\mathrm{Be})$ are both zero. However, these terms contribute numerically the largest amount to the difference between laboratory and solar neutrino release and will be calculated in Secs. III and IV.

In the following two subsections, I evaluate the neutrino energy using Eq. (2) for laboratory decays (in Sec. II A) and for solar decays (in Sec. II B). I discuss in Sec.

VII A the electrostatic energy of the screening cloud that surrounds the decaying nucleus.

A. Laboratory decays

The laboratory neutrino energy $q_{\rm lab}$ satisfies the equation

$$q_{\rm lab} + q_{\rm lab}^2/2M(^7{\rm Li}) = \Delta M + a_{\rm lab}(^7{\rm Be}) - a_{\rm lab}(^7{\rm Li}), \quad (4)$$

where the difference in atomic binding energies is

$$a_{\rm lab}(^7{\rm Be}) - a_{\rm lab}(^7{\rm Li}) = -0.195 \text{ keV}. \quad (5)$$

Since the energy difference between an initial and a final state is independent of the choice of steps used to reach the final state, the difference in atomic binding energies is equal to the difference between the sum of the successive ionization potentials of ^{7}Be and the sum of the successive ionization potentials of ^{7}Li. The difference in atomic binding energies given in Eq. (5) was calculated by subtracting the sum of the three ionization potentials of the lithium atom from the sum of the four ionization potentials of atomic beryllium, using the measured values for the ionization potentials [40].

Combining Eqs. (3) and (5) one obtains

$$m_e + M(^7{\rm Be}) - M(^7{\rm Li}) + a_{\rm lab}(^7{\rm Be}) - a_{\rm lab}(^7{\rm Li}) = 861.90 \text{ keV}, \quad (6)$$

which is the tabulated mass difference of the neutral atoms [27]. The small contribution of the ^{7}Li recoil energy is

$$q^2({\rm g.s.})/2M(^7{\rm Li}) \cong 0.057 \text{ keV}, \quad q^2({\rm e.s.})/2M(^7{\rm Li}) = 0.011 \text{ keV}, \quad (7)$$

for ground-state and excited-state transitions, respectively. Inserting Eqs. (6) and (8) in Eq. (4) we find the neutrino energies for the laboratory transitions,

$$q_{\rm lab}({\rm g.s.}) \cong 861.84 \text{ keV}, \quad (8)$$

and

$$q_{\rm lab}({\rm e.s.}) = 384.28 \text{ keV}, \quad (9)$$

that are shown in Fig. 1.

B. Solar decays

This subsection begins with a calculation of the neutrino energy that is released in the limiting case in which a continuum electron with zero kinetic energy is captured by a ^{7}Be nucleus at rest. I then calculate the neutrino energy that is emitted when a bound electron is captured from a stationary ^{7}Be nucleus. I evaluate the influence of nonzero kinetic energies of the electron and of the ^{7}Be ion in Secs. III and IV.

For the special case of continuum electron capture at rest, the neutrino energy release is the same as for laboratory capture except that the nucleus is assumed stripped of all bound electrons. Referring to Eq. (2), one can write

$$q_{\rm cont,star} = q_{\rm lab} - [a_{\rm lab}(^7{\rm Be}) - a_{\rm lab}(^7{\rm Li})]. \quad (10)$$

Therefore,

$$q_{\rm cont,star} = \Delta M - q_{\rm cont,star}^2/2M(^7{\rm Li}), \quad (11)$$

where the difference ΔM in rest mass energies is given by Eq. (3). Thus

$$q_{\rm cont,star}({\rm g.s.}) = 862.04 \text{ keV}. \quad (12)$$

I next consider the average neutrino energy that is released, $q_{\rm bound,star}$, when an electron is captured from a bound orbit. The only difference between $q_{\rm bound,star}$ and the previously calculated $q_{\rm cont,star}$ is the atomic binding energy of the electrons. Therefore, one can write

$$q_{\rm bound,star} = q_{\rm cont,star} + \langle a_{\rm star}(^7{\rm Be}) - a_{\rm star}(^7{\rm Li})\rangle, \quad (13)$$

where the angular brackets denote an average over the Sun. The K-shell binding energy has been determined for solar conditions by Iben and his collaborators [24] using a variational calculation. For the case in which one electron is bound to the ^{7}Be nucleus, the result can be expressed in terms of the relative K-shell binding, σ_R, in the Sun compared to the laboratory value, where σ_R is defined by the equation

$$a_{K,\rm star}(^7{\rm Be}) = -216.6\sigma_R \text{ eV}. \quad (14)$$

At the peak of the ^{7}Be solar neutrino emission, $\sigma_R \cong 0.25$ and $a_{K,\rm star}(^7{\rm Be}) = -0.06$ keV (cf. discussion in Sec. V). This binding energy is sufficiently small that it is not necessary, for our purposes, to calculate $a_{K,\rm star}(^7{\rm Be})$ to high precision. However, an accurate calculation was carried out without difficulty and the results of this calculation are described below. The average binding energies were obtained for two standard solar models [15] (see also Sec. V A): one that included, and one that did not include, helium diffusion. Using the tabulated results of the variational-principle calculation [24], a convenient interpolation formula was derived [35] for σ_R in terms of the local density, temperature, and chemical composition. Weighting the value of σ_R calculated at a given radial distance from the center of the Sun by the ^{7}Be neutrino flux at that radius, the average relative K-shell binding energy for the standard solar model [15] including helium diffusion is

$$\sigma_R \simeq 0.255, \quad (15)$$

and is 0.256 for the solar model that does not include helium diffusion. Thus, the average binding energy of a K-shell electron in the Sun is

$$\langle a_{K,\rm star}(^7{\rm Be})\rangle \cong -0.055 \text{ keV}. \quad (16)$$

The difference in atomic binding energies between two K-shell electrons in a beryllium atom in the Sun and a single K-shell electron in a lithium atom in the Sun may be estimated to more-than-adequate accuracy by scaling the K-shell energy given in Eq. (16) by the ratio of the square of the lithium and the beryllium nuclear charges. One can also estimate the energy difference by scaling (see [24]), using the same value of σ_R calculated above, the laboratory energy that is required to remove one electron from previously twice-ionized beryllium, leaving behind one electron bound to a lithium atom. Both methods give the same answer to the accuracy of interest here. One finds

$$\langle a_{2K,\mathrm{star}}(^7\mathrm{Be}) - a_{K,\mathrm{star}}(^7\mathrm{Li})\rangle \simeq -0.079 \text{ keV}. \quad (17)$$

One must average the results given in Eqs. (16) and (17) over the stellar model taking account of the variable fraction of the decays that occur from ^{7}Be atoms with one or with two bound electrons. Let p_1 and p_2 be the respective probabilities that ^{7}Be has one or two bound electrons that can decay by K capture. Then the appropriate average can be written as

$$\langle a\,(^7\mathrm{Be}) - a\,(^7\mathrm{Li})\rangle_{\mathrm{star}} = \left\langle \frac{p_1 a_{\mathrm{K,star}}\,(^7\mathrm{Be}) + 2p_2\left[a_{2K,\mathrm{star}}\,(^7\mathrm{Be}) - a_{2K,\mathrm{star}}\,(^7\mathrm{Li})\right]}{p_1 + 2p_2} \right\rangle. \quad (18)$$

Convenient expressions for p_1 and p_2 have been given by Iben and his collaborators [24]. Carrying out the average using the results for the relative ionization states obtained from the variational-principle calculation, I find for the atomic binding energy in the Sun:

$$\langle a(^7\mathrm{Be}) - a(^7\mathrm{Li})\rangle_{\mathrm{star}} = -0.06 \text{ keV}. \quad (19)$$

Inserting Eq. (19) in Eq. (13),

$$q_{\mathrm{bound,star}}(\mathrm{g.s.}) = 861.98 \text{ keV}. \quad (20)$$

By an analogous procedure, one can obtain the following results for the excited-state transition:

$$q_{\mathrm{cont,star}}(\mathrm{e.s.}) = 384.43 \text{ keV}, \quad (21)$$

and

$$q_{\mathrm{bound,star}}(\mathrm{e.s.}) = 384.38 \text{ keV}. \quad (22)$$

III. CAPTURE FROM CONTINUUM ORBITS

This section presents a calculation of the energy profile for the neutrino line emitted when electrons are captured from continuum orbits by ^{7}Be ions in the core of the Sun. The energy profile is the probability that a ^{7}Be ion captures an electron from the continuum and emits a neutrino of any specified energy. As noted earlier, continuum electron capture is the dominant process by which ^{7}Be nuclei decay in the solar interior [23]. The following section, Sec. IV, presents a calculation of the line profile when bound electrons are captured by ^{7}Be ions in the solar interior.

The partial transition probability to undergo electron capture can be written schematically, for a given relative flux density of electrons and ^{7}Be ions, as

$$d\lambda = \text{flux} \times \sigma_{\mathrm{cap}}, \quad (23)$$

where σ_{cap} is the appropriate weak interaction capture cross section. More specifically, the partial transition probability can be written in terms of the usual [41] charged-current β-decay Hamiltonian H_β as

$$d\lambda = 2\pi|\langle f|H_\beta|i\rangle|^2\delta\left(E_{\mathrm{initial}} - E_{\mathrm{final}}\right), \quad (24)$$

where the continuum wave functions are assumed to be normalized in a large, finite volume. Averaging over initial states, summing over final states, and integrating over all space, one obtains

$$\text{flux} \times d(\text{cross section}) = (2\pi)^{-2}\sum_f \overline{\sum_i}|\langle f|H_\beta|i\rangle|^2\delta^{(4)}(p_i - p_f)d^3\mathbf{q}d^3\mathbf{p}_7, \quad (25)$$

where the momenta in the final state of the neutrino and of the ^{7}Li ion are denoted by $\mathbf{q}$ and by $\mathbf{p}_7$, respectively. The β-decay Hamiltonian can be written as

$$H_\beta = 2^{-1/2}G\left[\bar{\psi}_\nu\gamma_\alpha\left(1+\gamma_5\right)\psi_e\right] \times \left[\bar{\psi}_n\gamma_\alpha\left(C_V - C_A\gamma_5\right)\psi_p\right], \quad (26)$$

where all the symbols have their usual meanings [41–43].

It is convenient to carry out the calculations in the center-of-momentum coordinate system. Relative to the laboratory frame in which the electron has a momentum $\mathbf{p}_e$ and the ^{7}Be ion has a momentum $\mathbf{p}_7$, the center-of-momentum frame has a velocity $\mathbf{V}$ given by

$$\mathbf{V} = M^{-1}\left(\mathbf{p}_e + \mathbf{p}_7\right), \quad (27)$$

where

$$M = m_e + M(^7\mathrm{Be}). \quad (28)$$

The equation describing the conservation of energy can be expressed simply in terms of the momentum $\mathbf{p}$ in the center-of-momentum frame, where $\mathbf{p}$ is given by

$$\mathbf{p} = M^{-1}\left[M(^7\mathrm{Be})\mathbf{p}_e - m_e\mathbf{p}_7\right]. \quad (29)$$

One can rewrite Eq. (2) in the form

$$E_{\mathrm{initial}} - E_{\mathrm{final}} = \Delta M + \frac{p^2}{2\mu} - q - \frac{q^2}{2M(^7\mathrm{Li})} = 0, \quad (30)$$

where the reduced mass μ is

$$\mu = \frac{m_e M(^7\mathrm{Be})}{m_e + M(^7\mathrm{Be})}. \tag{31}$$

The solution of Eq. (30) yields an expression for the neutrino energy in the center-of-momentum frame in terms of the momentum, p, of either of the particles, i.e.,

$$q \equiv q(p). \tag{32}$$

The β-decay matrix element in Eq. (25) can be greatly simplified by using the so-called "normal approximation" [41–43] that gives the leading term for the matrix element in a rapidly convergent power series expressed in terms of the small ($\lesssim 0.01$) quantities qR_{nucleus} and pR_{nucleus}, where R_{nucleus} is the nuclear radius of ^{7}Li. The conditions for the applicability of the normal approximation in stars are given in Eq. (10) of Ref. [43] and are satisfied to high accuracy in the present case.

Making the usual nonrelativistic reduction and summing over the spins of the nuclei in the initial and final states and over the spins of the electron and the neutrino, one finds in the center-of-momentum frame a simple expression for the product of the relative velocity of the particles times the capture cross section, namely,

$$v_{\mathrm{rel}}\sigma_{\mathrm{cap}} = \frac{G^2\xi|\psi_e|^2 q^2(p)}{2\pi\left[1 + q(p)/M(^7\mathrm{Li})\right]}, \tag{33}$$

where $|\psi_e|^2$ is the electron probability density (enhanced by the Coulomb attraction) averaged over the nucleus and ξ is the familiar sum of reduced matrix elements that occurs in allowed β decays [41–43], i.e.,

$$\xi = C_V^2\langle 1\rangle^2 + C_A^2\langle\sigma\rangle^2, \tag{34}$$

where $\langle 1\rangle$ and $\langle\sigma\rangle$ refer, respectively, to Fermi and Gamow-Teller matrix elements.

In a spherical shell at temperature T that contains $N(^7\mathrm{Be})$ total ^{7}Be ions, the rate at which ^{7}Be captures electrons is

$$d\ \mathrm{rate}(T) = N(^7\mathrm{Be})\langle n(e)\sigma_{\mathrm{cap}}v_{\mathrm{rel}}\rangle, \tag{35}$$

where the average that is indicated in Eq. (35) is over the thermal distributions of the electrons and the ^{7}Be ions. Writing out the thermal average explicitly, one finds

$$d\ \mathrm{rate}(T) = \frac{dV n(^7\mathrm{Be}) n(e) G^2\xi}{2\pi}\left(\frac{m_e}{2\pi kT}\right)^{3/2}\left(\frac{M(^7\mathrm{Be})}{2\pi kT}\right)^{3/2} \times \int\int d^3p_e d^3p_7 \exp\left(-p_e^2/2m_e kT\right)\exp\left[-p_7^2/2M(^7\mathrm{Be})kT\right]\frac{|\psi_e|^2 q^2(p)}{\left[1 + q/M(^7\mathrm{Li})\right]}, \tag{36}$$

where dV is the volume of the spherical shell and $n(e)$ and $n(^7\mathrm{Be})$ are, respectively, the local number density of electrons and of ^{7}Be ions. Converting the integration variables to the center-of-momentum quantities $\mathbf{p}$ and $\mathbf{P} = M\mathbf{V}$ [see Eqs. (27) and (29)], one obtains the relatively simple looking equation

$$d\ \mathrm{rate}(T) = C(T)\int\int d^3\mathbf{p} d^3\mathbf{P}\exp\left(-p^2/2\mu kT\right)\exp\left(-P^2/2MkT\right)\frac{|\psi_e|^2 q^2(p)}{\left[1 + q(p)/M(^7\mathrm{Li})\right]}, \tag{37}$$

where $C(T)$ is a constant that is independent of neutrino energy. To high accuracy in the present application, one can approximate the electron probability density by the nonrelativistic expression [41,43]

$$|\psi_e|^2 \cong \frac{8\pi\alpha v_e^{-1}}{1 - \exp\left(-8\pi\alpha v_e^{-1}\right)}, \quad v_e = \mu v_{\mathrm{rel}}/m_e, \tag{38}$$

where α is the fine structure constant and v_e is the velocity of the electron in the center-of-momentum frame.

The neutrino energy is measured in the laboratory frame, not in the center-of-momentum frame. Therefore, the rate of production of neutrinos of definite observed energies, q_{obs}, must be computed. The neutrinos that are observed experience a Doppler shift because of the motion $\mathbf{V}$ of the center-of-momentum frame relative to the laboratory frame. Let the z axis be oriented along the direction between the terrestrial detector and the core of the Sun. Then the nonrelativistic expression for the Doppler shift is

$$q_{\mathrm{obs}} = q_{\mathrm{c.m.}}(p)\left(1 - V_{z,\mathrm{c.m.}}\right), \tag{39}$$

which corresponds to a center-of-momentum velocity in the z direction of

$$V_{z,\mathrm{c.m.}} = \frac{P_z}{M} = \frac{q_{\mathrm{c.m.}}(p) - q_{\mathrm{obs}}}{q_{\mathrm{c.m.}}(p)}. \tag{40}$$

It is also convenient to introduce the relative energy in the center-of-momentum frame, i.e.,

$$E = \frac{p^2}{2\mu}. \tag{41}$$

The observed energy of the neutrino depends upon the direction in which the decaying nucleus is moving [via Eq. (39)], but only on the magnitude of the relative energy (not on the direction of $\mathbf{p}$): i.e.,

$$q_{\mathrm{c.m.}}(p) = q_{\mathrm{cont,star}} + p^2/2\mu = q_{\mathrm{cont,star}} + E. \tag{42}$$

Carrying out the integrations over the unimportant directions and converting from an integration over relative momentum to an integration over relative energy, one obtains

$$d\ \text{rate}(T) = C'(T) \int_0^\infty dE \int_{-\infty}^{+\infty} dP_z \exp(-E/T) \exp(-P_z^2/2MkT)$$
$$\times q_{\text{c.m.}}^2(E) \left[1 + q/M\left(^7\text{Li}\right)\right]^{-1} \left[1 - \exp\left(-8\pi\alpha m_e/p\right)\right]^{-1}. \quad (43)$$

The most important terms in Eq. (43) have direct physical interpretations. The function $\exp(-E/T)$ represents the Maxwell-Boltzmann distribution of relative internal energies E in the center-of-momentum frame and is dominated by the electron kinetic energy. The function $\exp(-P_z^2/2MkT)$ describes the Maxwell-Boltzmann distribution of the center-of-momentum velocities and is responsible for the Doppler shifts [via Eq. 39]. Since the ^{7}Be nucleus is much heavier than an electron, the center-of-momentum frame approximately coincides with the rest frame of the capturing ^{7}Be ion. Thus the velocities of the ^{7}Be nuclei essentially determine the Doppler shifts. The last three terms in Eq. (43) represent, respectively, the neutrino phase space (q^2), a small correction resulting from conservation of energy that is associated with the recoil energy of the ^{7}Li nucleus, and a small correction to the basically $1/v$ dependence [see Eq. (38)] of the probability density of the electron near the nucleus.

The exponent that describes the Doppler shift is

$$\frac{P_z^2}{2MkT} = \frac{M\left[q_{\text{obs}} - q_{\text{c.m.}}(E)\right]^2}{2kTq_{\text{c.m.}}^2(E)}, \quad (44)$$

which can be written in a convenient numerical form as

$$\frac{P_z^2}{2MkT} = \frac{51.023}{T_6} \frac{\left(q_{\text{obs}} - q_{\text{cont,star}} - E\right)^2}{\left(1 + E/q_{\text{cont,star}}\right)^2}, \quad (45)$$

where T_6 is the local temperature in the Sun measured in units of 10^6 K and the neutrino energy and the internal kinetic energy are expressed in keV. The large numerical coefficient in the exponent that is shown in Eq. (45) forces q_{obs} to be equal to $q_{\text{cont,star}} + E$ to within a fraction of a keV. Expressed in terms of the observed neutrino energy, Eq. (43) can be rewritten as

$$\frac{d\ \text{rate}\left(T, q_{\text{obs}}\right)}{dq_{\text{obs}}} = C'(T) \int_0^\infty dE\ \exp(-E/T) \exp\left(\frac{-51.023}{T_6} \frac{\left(q_{\text{obs}} - q_{\text{cont,star}} - E\right)^2}{\left(1 + E/q_{\text{cont,star}}\right)^2}\right)$$
$$\times q_{\text{c.m.}}^2(E) \left[1 + q/M\left(^7\text{Li}\right)\right]^{-1} \left[1 - \exp\left(-8\pi\alpha m_e/p\right)\right]^{-1}, \quad (46)$$

which is the principal result of this section.

The normalized spectrum of neutrino energies due to electron capture from continuum orbits within a spherical shell at temperature T is

$$\text{spectrum}_{\text{cont}}\left(T, q_{\text{obs}}\right) = \frac{d\ \text{rate}\left(T, q_{\text{obs}}\right)/dq_{\text{obs}}}{\sum_{q_{\text{obs}}} d\ \text{rate}\left(T, q_{\text{obs}}\right)/dq_{\text{obs}}}. \quad (47)$$

The average over spherical shells at different temperatures will be described in Sec. V, where use will be made of detailed solar models.

IV. CAPTURE FROM BOUND ELECTRON ORBITS

A small, but significant fraction of electron captures in the Sun occur from bound orbits. This section describes the calculation of the neutrino energy profile for bound electron captures. The rate of bound capture in the Sun was first evaluated by Iben and his collaborators [24] in an elegant paper which carried out a variational-principle calculation of the binding energies and eigenfunctions in the presence of the solar plasma and which also presented formulas for the fractional occupation of different bound atomic levels as a function of the ambient physical variables.

The normalized energy profile resulting from bound capture has the simple form

$$\text{spectrum}_{\text{bound}}\left(q_{\text{obs}}, T\right) = q_{\text{bound,star}}^{-1} \left(\frac{M(^7\text{Be})c^2}{2\pi kT}\right)^{1/2} \exp\left[-\frac{M(^7\text{Be})c^2}{2kT}\left(\frac{q_{\text{obs}} - q_{\text{bound,star}}}{q_{\text{bound,star}}}\right)^2\right], \quad (48)$$

where $q_{\rm bound,star}$ is given in Eqs. (20) and (22). The spectrum given by Eq. (48) is obtained directly from the Maxwell-Boltzmann distribution for the ^{7}Be ions by substituting for P_z the expression given in Eq. (40) for the ion momentum. For the capture of bound electrons, the center-of-momentum frame coincides with the rest frame of the ^{7}Be ion, which is why the kinematic complications that are present for the case of continuum capture (in which both electrons and ^{7}Be ions have nonzero translational velocities) are absent for bound capture.

The fraction, $f_{\rm bound}/(1.0+f_{\rm bound})$, of electron captures that occur from bound K-shell orbits of ^{7}Be at a fixed temperature is given by the expression [24]

$$f_{\rm bound}(T) = (5.07/T_6)\, S_R \exp\left(2.515\sigma_R/T_6\right), \qquad (49)$$

where S_R and σ_R are quantities that result from the variational principle calculation. Bahcall and Moeller [35] have given a convenient formula for σ_R [see Eq. (14) for the definition of σ_R]. They give

$$\sigma_R \cong -0.431 + 2.091r - 1.481r^2 + 0.401r^3 , \qquad (50a)$$

in terms of the dimensionless Debye-Huckel screening length r (the Debye-Huckel screening length divided by the Bohr radius), where

$$r = 0.298\left[64T_6/\rho\,(3+X)\right]^{1/2} , \qquad (50b)$$

with ρ and X being, respectively, the local density (in g cm^{-3}) and the hydrogen mass fraction. The quantity S_R can be calculated from formulas given in [24], i.e.,

$$S_R = C_R^2 D^{-1}\left[1 + 0.435 L_R \exp\left(-0.735\sigma_R/T_6\right)\right] , \qquad (50c)$$

$$D = \left[1 + L_R + 0.25 L_R^2 \exp\left(-0.735\sigma_R/T_6\right)\right] , \qquad (50d)$$

$$L_R = 0.246\left(\rho\mu_e^{-1}T_6^{-3/2}\right)\exp\left(2.515\sigma_R/T_6\right) , \qquad (50e)$$

where μ_e is the electron mean molecular weight, and [35]

$$C_R^2 \cong -0.6064 + 4.859r - 5.283r^2 + 1.907r^3 . \qquad (50f)$$

The bound enhancement, $f_{\rm bound}$, averaged over the conditions of a standard solar model yields a value of $f_{\rm bound} \approx 0.21$ [35] (see also column 5 of Table III of this paper).

V. CHARACTERISTICS OF THE ENERGY PROFILE

This section describes the characteristics of the energy profiles of the two ^{7}Be neutrino lines that are shown in Fig. 1. The calculated profiles have been averaged over the physical parameters of detailed solar models. The discussion makes use of the energy spectra that were computed for fixed temperatures in Sec. III for electron captures from continuum orbits [see especially Eqs. (43) and (47)] and in Sec. IV for captures from bound orbits [see especially Eqs. (48) and (49)].

The energy spectra are given numerically in Tables I and II. The most striking characteristic of the line profiles is their asymmetry. Figures 2 and 3 display the calculated line profiles. The characteristic shapes, above and below the energy at which the probability for neutrino emission is a maximum, will be explained physically and derived analytically (approximately) in the following section, Sec. VI.

The basic properties of the line profile that are computed numerically in this section are the shift in average neutrino energy, Δ, relative to the laboratory energy of the neutrino line, the full-width-at-half-maximum (FWHM) of the line profile, the half-width at half-maximum for energies above (W_+) and below (W_-) the peak of the line profile, and the first, second, and third moments of the energy distributions. For all the solar models that are described in Table III, these characteristics of the energy profile are given in Table V for both ground-state capture (862 keV, see Fig. 1) and excited-state capture (384 keV, see Fig. 1).

A. Solar models

The principal characteristics of the four solar models [14,15,44] that were used to compute the averaged line profiles are summarized in Table III. The preferred solar model, which is listed first in both Tables III and V, was

TABLE III. Some characteristics of four standard solar models.

Model	Shells ($T > 6\times10^6$ K)	$T_{\rm central}$ (10^6 K)	$\langle T\rangle$ (Weight: ^{7}Be)	Bound fraction (^{7}Be decays)	$\phi(^7{\rm Be})$ (10^9 cm^{-2}s^{-1})	$\phi(^8{\rm B})$ (10^6 cm^{-2}s^{-1})
Bahcall-Pinsonneault 1992 (helium diffusion)	127	15.67	14.13	0.215	4.9	5.7
Bahcall-Pinsonneault 1992 (no diffusion)	127	15.57	14.06	0.217	4.6	5.1
Bahcall-Ulrich 1988 (no diffusion)	87	15.64	14.07	0.219	4.7	5.8
Bahcall *et al.* 1982 (no diffusion)	19	15.50	13.6	0.226	4.3	5.6

computed by Bahcall and Pinsonneault [15] and is the only detailed solar interior model published to date that includes helium diffusion. For comparison, I calculate the line profile with a model labeled (no diffusion) that was computed [15] with the same input data that was used in calculating the preferred model, except that the "no diffusion" model does not include helium diffusion. As a test of the robustness of the results, I have also calculated the energy profiles with the aid of standard solar models computed earlier, in 1988 [14] and in 1982 [44], which used less accurate input data. Note that the number of spherical shells used in the interior region in which ^{7}Be neutrinos are produced increases monotonically from 19 shells used in the 1982 solar model to 127 shells used in the 1992 models. The results given below show that there are no significant differences among the line profiles computed with the three high-resolution models (with interior shells ≥ 87).

The solar models listed in Table III span a decade of state-of-the-art solar research. All four models have the same central temperature to within $\pm 0.5\%$:

$$T_c = (15.58 \pm 0.08) \times 10^6 \text{ K}. \quad (51)$$

The central temperature for the three more-precise models varies over a range of $\pm 0.3\%$. The less accurate 1982 model has a central temperature that differs by 0.8% from the average modern value.

The average temperature $\langle T \rangle_{^7\text{Be}}$ computed by weighting the temperature in each spherical shell according to the ^{7}Be neutrino flux produced in that shell,

$$\langle T \rangle_{^7\text{Be}} = \sum_T d\phi \left(^7\text{Be}, T \right) T, \quad (52)$$

is the same to within $\pm 0.3\%$ for the three solar models from 1988 and 1992, i.e.,

$$\langle T \rangle_{^7\text{Be}} = (14.10 \pm 0.04) \times 10^6 \text{ K}. \quad (53)$$

The 1982 model has a ^{7}Be-weighted temperature of $\langle T \rangle_{^7\text{Be}} = 13.6 \times 10^6$ K, which differs by about 3.5% from the more accurate later models, presumably because of the small number of shells (19) (used in the earlier calculation). The variation over the past decade in the computed total ^{7}Be neutrino flux is $\pm 6\%$; the decadal variation in the computed ^{8}B neutrino flux is also $\pm 6\%$.

The relative number of electron captures that occur from bound orbits f_{bound} is robustly determined by the solar models. From Table III,

$$f_{\text{bound}} = 0.221 \pm 0.006. \quad (54)$$

This result is in good agreement with the 1969 value [35] of $f_{\text{bound}} = 0.21$.

Table IV lists the central temperatures for ten other recently published solar models that were calculated by different groups using different computer codes and different input parameters [45], as well as the 1988 and 1992 (no-diffusion) solar models described in Table III. None of the solar models listed in Table IV includes helium diffusion. The heterogeneous set of models referred to in Table IV were derived for a variety of different applications, most of which were not directly related to solar neutrinos. The applications often did not require the highest-obtainable accuracy for the solar interior conditions. The precision with which the models were constructed and the accuracy of the input data varies from model to model. In many cases, the authors did not use the best-available radiative opacities and nuclear reaction rates. The central temperatures given by the variety of solar models listed in Table IV can be summarized by the relation

TABLE IV. Central temperatures of 12 recently computed solar models (no diffusion).

Model	T_c (10^6 K)
Castellani, Degl'Innocenti, and Fiorentini 1993	15.72
Berthomieu *et al.* 1993	15.55
Turck-Chièze and Lopes 1993	15.43
Ahrens, Stix, and Thorn 1992	15.65
Bahcall and Pinsonneault 1992	15.57
Christensen-Dalsgaard 1992	15.68
Guenther *et al.* 1992	15.53
Guzik and Cox 1991	15.40
Proffitt and Michaud 1991	15.71
Sackmann *et al.* 1990	15.43
Bahcall and Ulrich 1988	15.64
Lebreton and Däppen 1988	15.54

$$T_{\text{central}}(\text{no diffusion}) = 15.55(1 \pm 0.01) \times 10^6 \text{ K}. \quad (55)$$

All of the central temperatures in Table IV would be increased by $\simeq 0.1 \times 10^6$ K if diffusion were included.

Taken together, the results shown in Tables III and IV demonstrate that the central temperature of the Sun is determined to $\pm 1\%$ even without requiring unusual precision and accuracy in the calculations. In what follows, I shall only make use of the four solar models listed in Table III, since these are the only models, with which I am acquainted, whose characteristics are published in sufficient detail to permit precise calculations of the ^{7}Be line profile.

B. Properties of the energy spectrum

The neutrino energy spectrum that is produced in a spherical shell of the Sun that is at a specified temperature T is obtained by adding the normalized energy spectra for the capture of electrons from continuum orbits (computed in Sec. III) and the normalized spectrum from bound orbits (computed in Sec. IV). The relative contributions are weighted by the factor f_{bound} that was defined in Eq. (49). Thus

$$\text{spectrum}\,(T, q_{\text{obs}}) = \frac{\text{spectrum}_{\text{cont}}\,(T, q_{\text{obs}}) + f_{\text{bound}}(T)\text{spectrum}_{\text{bound}}\,(T, q_{\text{obs}})}{1 + f_{\text{bound}}(T)}. \quad (56)$$

The neutrino spectrum for the entire Sun predicted by a particular solar model is the weighted average of spectrum (T, q_{obs}), weighted with respect to the ^{7}Be flux that is produced at each temperature. Therefore, the neutrino spectrum predicted by a given solar model is

$$\text{spectrum}_{\text{solar}}\,(q_{\text{obs}}) = \sum_T d\phi\left(^7\text{Be}, T\right)\text{spectrum}\,(T, q_{\text{obs}})\,, \quad (57)$$

where the ^{7}Be neutrino flux is normalized to unity when integrated over the whole star:

$$\sum_T d\phi\left(^7\text{Be}, T\right) = 1.000. \quad (58)$$

The values of the weighting factors, $d\phi\left(^7\text{Be}, T\right)$, are given in published tables [14,15,44] for all four of the models used here. The numerical values for $\text{spectrum}_{\text{solar}}(q_{\text{obs}})$ are given in Tables I and II.

The predicted probability distribution for the neutrino energy spectrum has a maximum at a well-defined energy q_{peak} whose location is obvious in Figs. 2 and 3. The peak of the probability distribution exceeds by a small amount δq [see Eqs. (10) and (12)], the neutrino energy $q_{\text{cont,star}}$ that corresponds to capturing an electron from a continuum orbit with zero kinetic energy, i.e.,

$$\delta q \equiv q_{\text{peak}} - q_{\text{cont,star}}. \quad (59)$$

For the most accurate available standard solar model, which is labeled "Bahcall-Pinsonneault 1992 (helium diffusion)" in Tables III and V, the shift δq for the (more energetic) ground-state transition is

$$\delta q\ (\text{g.s.}) = 0.23\ \text{keV}, \quad (60)$$

and is

$$\delta q\ (\text{e.s.}) = 0.04\ \text{keV} \quad (61)$$

for the (less energetic) excited-state transition. Essentially identical values of δq are obtained with the other solar models used here (see the last column of Table V). The value of q_{peak} can be calculated using the last column of Table V and the relation given in Eq. (59), i.e.,

$$q_{\text{peak}} = q_{\text{cont,star}} + \delta q. \quad (62)$$

The value of q_{peak} for ground-state transitions is

$$q_{\text{peak}}\ (\text{g.s.}) = (862.27 \pm 0.01)\ \text{keV}\,, \quad (63)$$

0.43 keV larger than the laboratory decay energy (see Sec. II A). For excited-state decays, the energy peak occurs at

$$q_{\text{peak}}\ (\text{g.s.}) = (384.47 \pm 0.01)\ \text{keV}, \quad (64)$$

0.19 keV larger than the laboratory decay energy (Sec. II A).

It is convenient to define the nth moment of the solar energy spectrum by the relation

TABLE V. Characteristics of the energy profile.

Model	Δ (keV)	$\langle q - q_{\text{peak}}\rangle$ (keV)	FWHM (keV)	W_- (keV)	W_+ (keV)	$\langle (q - q_{\text{peak}})^2\rangle$ (keV)	$\langle (q - q_{\text{peak}})^3\rangle$ (keV)	δq (keV)
			Ground-state decay					
Bahcall-Pinsonneault 1992 (helium diffusion)	1.29	0.856	1.63	0.56	1.07	2.59	10.0	0.23
Bahcall-Pinsonneault 1992 (no diffusion)	1.28	0.858	1.62	0.55	1.07	2.58	9.9	0.22
Bahcall-Ulrich 1988 (no diffusion)	1.28	0.857	1.62	0.55	1.07	2.58	9.9	0.22
Bahcall *et al.* 1982 (no diffusion)	1.23	0.821	1.56	0.53	1.03	2.39	8.8	0.21
			Excited-state decay					
Bahcall-Pinsonneault 1992 (helium diffusion)	1.24	1.048	0.97	0.24	0.73	2.86	11.3	0.04
Bahcall-Pinsonneault 1992 (no diffusion)	1.23	1.040	0.96	0.24	0.72	2.82	11.1	0.04
Bahcall-Ulrich 1988 (no diffusion)	1.23	1.039	0.95	0.24	0.71	2.82	11.1	0.04
Bahcall *et al.* 1982 (no diffusion)	1.18	1.002	0.91	0.22	0.69	2.62	9.9	0.03

$$\langle (q - q_{\rm peak})^n \rangle \equiv \int_0^\infty dq\, {\rm spectrum}_{\rm solar}(q)\, (q - q_{\rm peak})^n \,. \tag{65}$$

The moments are computed about the energy $q_{\rm peak}$ at which the probability distribution peaks.

The shift in average neutrino energy, Δ, from the laboratory value to the solar interior value is

$$\Delta \equiv \left\langle q - q_{\rm lab} \right\rangle, \tag{66}$$

or, using the definition of the spectrum moments given in Eq. (65),

$$\Delta = \left\langle q - q_{\rm peak} \right\rangle + (q_{\rm peak} - q_{\rm cont,star}) + (q_{\rm cont,star} - q_{\rm lab}) \,. \tag{67}$$

The first two terms in Eq. (67) are given in columns 3 and 9 of Table V. The last term can be computed from Eqs. (8), (9), (12), and (21) of Sec. II. The value of $(q_{\rm cont,star} - q_{\rm lab})$ is 0.20 keV for ground-state transition and 0.15 keV for excited-state transition. Combining the results given in Table V, the shift for the ground-state transition is, for all three of the modern (1988–1992) models,

$$\Delta \text{ (g.s.)} = 1.29 \text{ keV}, \tag{68}$$

with a spread of only $\pm 0.5\%$. The earlier (1982) model yields Δ(g.s.) = 1.23 keV. The shift for the excited-state transition is

$$\Delta \text{ (e.s.)} = 1.24 \text{ keV} \tag{69}$$

for the three modern models with a spread of only $\pm 0.5\%$. The earlier (1982) model gives a 4% smaller value, 1.18 keV.

Table V also presents some of the other calculated characteristics of the energy profile. The full-width-at-half maximum of the profile is denoted by FWHM and is listed in column 4 of Table V; the half-width on the low-energy side of the peak (column 5) is denoted by W_- and the half-width on the high-energy side (column 6) is denoted by W_+. The most accurate values for the ground-state transition are

$$\text{FWHM (g.s.)} = 1.63 \text{ keV} \,, \; W_-\text{(g.s.)} = 0.56 \text{ keV} \,, \; W_+\text{(g.s.)} = 1.07 \text{ keV}. \tag{70}$$

The corresponding values for the excited-state transition are

$$\text{FWHM (e.s.)} = 0.97 \text{ keV} \,, \; W_-\text{(e.s.)} = 0.24 \text{ keV} \,, \; W_+\text{(e.s.)} = 0.73 \text{ keV} \,. \tag{71}$$

Figures 2 and 3 are remarkably asymmetric. The degree of asymmetry can be quantified by taking the appropriate dimensionless ratio of the third and the second moments that is known as the skewness. For our case, the skewness of the profile is given by

$$\text{skewness} \equiv \frac{\langle (q - q_{\rm peak})^3 \rangle^2}{\langle (q - q_{\rm peak})^2 \rangle^3}. \tag{72}$$

The values of the skewness that are computed from columns 7 and 8 of Table V are, respectively,

$$\text{skewness (g.s.)} = 5.7 \,, \; \text{skewness (e.s.)} = 5.5 \,. \tag{73}$$

The skewness of any symmetric distribution, such as the normal distribution, is equal to zero.

The shape of the energy profile can be well described by simple analytic functions. For neutrino energies less than the peak energy, the profile is essentially Gaussian, i.e.,

$$\text{spectrum}_{\rm solar}(q_{\rm obs}) \cong N \exp\left[-(q_{\rm obs} - q_{\rm peak})^2 / 2w^2 \right] \,, \quad q_{\rm obs} < q_{\rm peak}. \tag{74}$$

The high-energy tail is well described by a Boltzmann distribution, i.e.,

$$\text{spectrum}_{\rm solar}(q_{\rm obs}) \cong N \exp\left[-(q_{\rm obs} - q_{\rm peak}) / T_{\rm eff} \right] \,, \quad q_{\rm obs} > q_{\rm peak}. \tag{75}$$

In Eqs. (74) and (75), the quantity N is a normalization factor. For ground-state capture, the effective width, w, to be used in Eq. (74) is approximately

$$w\text{(g.s.)} = 0.48 \text{ keV} \,. \tag{76a}$$

The corresponding value for excited-state capture is

$$w\text{(e.s.)} = 0.20 \text{ keV} \,. \tag{76b}$$

Both transitions are well described by a single effective temperature,

$$kT_{\rm eff} = 1.31 \pm 0.02 \text{ keV} \,, \tag{77a}$$

i.e.,

$$T_{\rm eff} \cong 15.1 \times 10^6 \text{ K}. \tag{77b}$$

The uncertainty indicated in the value of the effective temperature $T_{\rm eff}$ reflects the fact that Eq. (75) is only approximate and the best-fitting value of $T_{\rm eff}$ varies somewhat with neutrino energy.

VI. APPROXIMATE ANALYTIC DERIVATIONS OF THE ENERGY SHIFT AND ENERGY PROFILE

This section gives approximate analytic derivations of the principal characteristics of the neutrino energy spectrum from ^{7}Be electron capture in the Sun. The purpose of this discussion is to provide insight regarding the physical origins of the profiles that are shown in Figs. 2 and 3. For simplicity, I will usually concentrate on the profile created at a fixed temperature T_6 ignoring the average over the temperature distribution of the center of the Sun. In some cases, I will also ignore the small (20%) contribution to the energy profile that arises from captures from bound states (cf. discussion in Sec. IV). In

all cases, I will omit small terms of order $q/M(^7\mathrm{Li})$, the ratio of the neutrino energy q to the mass of the ^{7}Li nucleus, and terms of order E/q, the ratio of the relative kinetic energy E of the electron and of the nucleus to the neutrino energy.

These approximations permit the isolation of the principal physical processes that determine the neutrino energy profile and allow analytic calculations to be made that reproduce the general features of the detailed numerical results.

I begin by deriving approximate expressions for the energy half-widths W_- and W_+ and then obtain an analytic expression for the energy shift Δ.

A. Energy half-widths

The low-energy side of the profile, $q_{\mathrm{obs}} < q_{\mathrm{peak}}$, is produced by ^{7}Be nuclei that are moving away from the observer and which capture electrons with small or zero kinetic energies (i.e., low-velocity electrons from the continuum or electrons in bound orbits). For such captures, the reaction rate is given approximately by [see Eqs. (43), (45), and (48)]

$$d\ \text{rate} \ \propto\ \text{const} \times \exp\left[-\frac{51}{T_6}\left(q_{\mathrm{obs}} - q_{\mathrm{cont,star}} - \delta q\right)^2\right]. \tag{78}$$

Replacing in Eq. (78) the expression $(q_{\mathrm{obs}} - q_{\mathrm{cont,star}} - \delta q)$ by W_-, the half-width-at-half maximum on the low-energy side, one has

$$W_- \approx \left(\ln 2 \langle T_6 \rangle / 51\right)^{1/2}. \tag{79}$$

Evaluating Eq. (79) for a characteristic ^{7}Be temperature of 14×10^6K (see discussion of solar models in Sec. V A) yields

$$W_- \approx 0.44\ \text{keV}. \tag{80}$$

This result is in satisfactory agreement with the low-energy width that is calculated numerically, $W_- = 0.56$ keV (see Table V).

The high-energy side of the profile, $q_{\mathrm{obs}} > q_{\mathrm{peak}}$, is produced by electrons and ^{7}Be nuclei with significant internal kinetic energies E [see Eq. (43)]. Since the product of the separate Boltzmann distributions for the electrons and for the ^{7}Be ions is a Boltzmann distribution in the center-of-momentum frame, the high-energy part of the profile has the approximate shape

$$d\ \text{rate} \propto\ \text{const} \times \exp(-E/T)\ , \tag{81}$$

where

$$E = p^2/2\mu, \tag{82}$$

and the relative momentum p is defined by Eq. (29). One can define an effective temperature, T_{eff}, for the high-energy tail of the spectrum by fitting at two energies the expression given in Eq. (81) to the numerically computed energy spectra that are given in Tables I and II (and shown in Figs. 3 and 4). Symbolically,

$$T_{\mathrm{eff}} \approx \frac{q_{\mathrm{obs}}(2) - q_{\mathrm{obs}}(1)}{\ln\left[\mathrm{spectrum}_{\mathrm{obs}}(q_{\mathrm{obs}}(1))/\mathrm{spectrum}_{\mathrm{obs}}(q_{\mathrm{obs}}(2))\right]}, \tag{83}$$

where $q_{\mathrm{obs}}(1)$, $q_{\mathrm{obs}}(2)$ are typical energies in the line profile. The value of T_{eff} depends slightly on the choice of $q_{\mathrm{obs}}(1)$, $q_{\mathrm{obs}}(2)$. For both transitions shown in Fig. 1,

$$T_{\mathrm{eff}} \cong 1.31\ \text{keV} \approx 15 \times 10^6\ \text{K}, \tag{84}$$

which translates into a half-width-at-half-maximum of

$$W_+ \cong (\ln 2) T_{\mathrm{eff}} \approx 0.91\ \text{keV}. \tag{85}$$

The value for W_+ given in Eq. (85) is approximately halfway between the accurate values given in Table V for the ground-state decay (1.07 keV) and the excited-state decay (0.73 keV).

The reason that the effective temperature given in Eq. (84) is slightly larger than the value obtained from the solar model and given in Eq. (53) is that Eq. (83) is only approximate. A more accurate (but less transparent) determination of T_{eff} can be obtained by taking the ratio of integrand in Eq. (46) at two neutrino energies and setting that ratio equal to the ratio of the spectrum probabilities. This more accurate relation should be used in interpreting future experiments.

B. The energy shift: Δ

The energy shift Δ can be written as the sum of two terms: $\langle q_{\mathrm{obs}} - q_{\mathrm{cont,star}} \rangle$ plus $(q_{\mathrm{cont,star}} - q_{\mathrm{lab}})$ [cf. Eq. (67)]. For the ground-state transition, $(q_{\mathrm{cont,star}} - q_{\mathrm{lab}})$ is 0.20 keV and is 0.15 keV for the excited-state transition [see discussion in Secs. II and V B following Eq. (67)]. The dominant term in the energy shift, $\langle q_{\mathrm{obs}} - q_{\mathrm{cont,star}} \rangle$, is equal (to numerical accuracy, which is better than 1%) to the same value, 1.09 keV, for both ground-state and excited-state transitions. This numerical equality can be established as follows. The quantity $\langle q_{\mathrm{obs}} - q_{\mathrm{cont,star}} \rangle$ is equal to the sum of two terms, $\langle q_{\mathrm{obs}} - q_{\mathrm{peak}} \rangle + \delta q$, both of which are given in Table V. Adding the two terms in Table V gives, for all of the solar models, essentially identical values for $\langle q_{\mathrm{obs}} - q_{\mathrm{cont,star}} \rangle$.

At first sight, it is surprising that the energy shift relative to $q_{\mathrm{cont,star}}$, $\langle q_{\mathrm{obs}} - q_{\mathrm{cont,star}} \rangle$, is independent of the value of $q_{\mathrm{cont,star}}$. However, a simple analytic argument, given below, shows that, at a specified temperature T, the shift $\langle q_{\mathrm{obs}} - q_{\mathrm{cont,star}} \rangle_T$ is, to an excellent approximation, the mean kinetic energy of the electron and the ^{7}Be nucleus that interact to produce the electron capture reaction. The mean kinetic energy is, of course, independent of $q_{\mathrm{cont,star}}$.

The average value of the shift relative to $q_{\mathrm{cont,star}}$ is

$$\langle q_{\rm obs} - q_{\rm cont,star}\rangle_T = \int_0^\infty dq_{\rm obs}\,(q_{\rm obs} - q_{\rm cont,star})\ {\rm spectrum}_T(q_{\rm obs}), \tag{86}$$

which can be rewritten approximately using Eqs. (43) and (44) as

$$\langle q_{\rm obs} - q_{\rm cont,star}\rangle_T \cong T^{-1}\left(\frac{\beta\pi}{q^2_{\rm cont,star}}\right)^{1/2}\int_0^\infty dE\ \exp(-E/T) \times \int_{-\infty}^{+\infty} dq_{\rm obs}\,(q_{\rm obs} - q_{\rm cont,star})\ \exp\left[-\beta\,(q_{\rm obs} - q_{\rm cont,star} - E)^2/q^2_{\rm cont,star}\right]. \tag{87}$$

The key fact that simplifies Eq. (87) and results in the equality of the energies for ground-state and excited-state transitions is that the quantity β, which appears in the second exponent in Eq. (87), is very large. Equations (44) and (45) show that β is just the ratio of the nuclear rest mass energy (~ 7 GeV) to the ambient temperature (~ 1 keV), i.e.,

$$\beta = \frac{Mc^2}{2kT} \gg 1. \tag{88}$$

In the limit of large β,

$$(\beta/\pi)^{1/2}\ \exp\left(-\beta x^2\right) \underset{\beta\to\infty}{\longrightarrow} \delta(x), \tag{89}$$

which greatly simplifies Eq. (87). The effect of the delta function is to enforce energy conservation independent of the Doppler shifts, i.e.,

$$q_{\rm obs} - q_{\rm cont,star} = E. \tag{90}$$

Carrying out the integration over the delta function gives

$$\langle q_{\rm obs} - q_{\rm cont,star}\rangle_T \cong T^{-1}\int_0^\infty dE E\ \exp\,(-E/T) = T. \tag{91}$$

Therefore,

$$\langle q_{\rm obs} - q_{\rm cont,star}\rangle_\odot \cong \int_\odot dTTd\phi\left(^7{\rm Be}, T\right) = 1.2\ {\rm keV}, \tag{92}$$

which is, as promised, independent of $q_{\rm cont,star}$.

VII. OTHER EFFECTS

This section shows that the effects on the neutrino energy profile of electrostatic screening energy (Sec. VII A), of the gravitational redshift (Sec. VII B), and of collisional broadening (Sec. VII C) are much smaller than the dominant terms (calculated in Secs. III–V) that arise directly from the Maxwellian energy distributions of the electrons and of the ions.

A. Electrostatic screening energy

There is a difference in electrostatic screening energy between the initial and final states of ^{7}Be continuum electron capture. In the initial state, a ^{7}Be nucleus (charge $z = 4e$) and a nearby electron jointly interact electrostatically with a surrounding charge cloud of electrons and ions that screen the nucleus. After the electron is captured, only the nuclear Coulomb potential corresponding to a charge $z = 3e$ interacts with the screening cloud. The difference in electrostatic screening energy is contributed partly to the energy of the emitted neutrino.

The electrostatic screening energy $\delta E_{\rm Coul}$ can be estimated by generalizing the familiar Debye-Huckel calculation of the charge distribution and the potential associated with the monopole field of a single ion. The more general case consists of a monopole field (from the capturing ion) plus a dipole field (from the ion plus the electron that is about to be captured). Solving Poisson's equation for the monopole plus dipole fields, one obtains the potential $\phi_{\rm before}\,(\mathbf{r})$ before the electron capture occurs,

$$\phi_{\rm before}\,(\mathbf{r}) = z_{\rm net}\frac{\exp(-\kappa r)}{r} + \frac{p\kappa}{r}\exp(-\kappa r)\left[1 + (\kappa r)^{-1}\right]\cos\Theta, \tag{93}$$

where κ is the inverse of the Debye-Huckel screening length:

$$\kappa^2 = 4\pi e^2 T^{-1}\Sigma_i z_i^2 n_i. \tag{94}$$

The first term on the right-hand side of Eq. (93) is the standard Debye-Huckel potential for a point charge, $z_{\rm net}$, surrounded by a screening cloud, where the net (point) charge in the present case is $+3e$. The second term is the dipole solution in which p is the dipole moment produced by the ^{7}Be nucleus and the (to-be-captured) electron. In the usual approximation that the screening potential is smaller than the thermal energy, the charge density surrounding the ^{7}Be nucleus and the electron is

$$\rho_{\rm before}\,(\mathbf{r}) = -\frac{\kappa^2}{4\pi}\phi_{\rm before}\,(\mathbf{r}). \tag{95}$$

The Coulomb energy both before and after the electron capture can be evaluated from the relation

$$E_{\rm Coul} = \tfrac{1}{2}\int d^3\mathbf{r}\rho(\mathbf{r})\phi(\mathbf{r}). \tag{96}$$

In evaluating the initial Coulomb energy, the potential and the charge distribution are taken from Eqs. (93) and (94). One may approximate the final Coulomb energy by assuming that the density distribution of the charge

cloud is unchanged immediately after the electron capture occurs, but that the final potential only includes a pure monopole term ($3e/r$) due to the final nucleus plus the potential due to the screening charges. The potential due to the screening charges can be taken from the defining relation

$$\phi_{\rm before}\ (\mathbf{r}) \equiv \phi_{\rm screening}\ (\mathbf{r}) + \frac{3e}{r} + \frac{p}{r^2}\cos\Theta. \qquad (97)$$

The difference in Coulomb energies, $\delta E_{\rm Coul}$, obtained in this way is

$$\delta E_{\rm Coul} \approx -\frac{4}{15}\frac{e^2}{R_D}\left(\frac{\lambda\!\!\!^{-}_D}{R_D}\right), \qquad (98)$$

where $\lambda\!\!\!^{-}_D$ is the de Broglie wavelength of the electron and $R_{\rm DH} = \kappa^{-1}$ is the Debye-Huckel screening length. In obtaining Eq. (98), I evaluated the dipole moment by assuming that the electron and the ^{7}Be nucleus are separated by a distance $\lambda\!\!\!^{-}_D$ with the origin at the center of charge. This yields $p = 8e\lambda\!\!\!^{-}_D/5$. Inserting typical solar-interior values into Eq. (98), one finds

$$\delta E_{\rm approx\ Coul} \approx -0.004\ \ {\rm keV}. \qquad (99)$$

One can obtain a conservative upper limit to the change in electrostatic screening energy by assuming that the electron is far away from the nucleus when the electron is captured. In this extreme limit, one can approximate the change in Coulomb energy by

$$E_{\rm Coul} = \tfrac{1}{2}\int d^3\mathbf{r}\rho(\mathbf{r})_{Z=4}\left[\phi(\mathbf{r})_{Z=4} - \phi(\mathbf{r})_{Z=3}\right], \qquad (100)$$

where in writing Eq. (100) it was also assumed that the particles in the screening cloud around the ^{7}Be nucleus do not have time to move during the electron capture. These assumptions yield

$$\delta E_{\rm extreme\ Coul} \approx -\frac{e^2}{R_D} \simeq -0.065\ \ {\rm keV}. \qquad (101)$$

Some fraction, $\epsilon < 1$, of the Coulomb energy difference represented by Eq. (99) or (101) should be added to the neutrino energies calculated in the previous sections. This addition is estimated to lie between 0.004ϵ keV and 0.065ϵ keV, which is a rather small effect. However, a quantum mechanical calculation of the change in electrostatic screening energy would be of interest.

B. Gravitational redshift

Each neutrino energy is shifted by an amount Δq,

$$\Delta q({\rm GR}) = \frac{-GM(\leq r)}{rc^2}q, \qquad (102)$$

due to the general relativistic redshift. In the region in which the neutrinos are produced, the mean shift $\Delta q/q \approx 10^{-5}$ [28]. Therefore, the average change in the neutrino energy is only

$$\Delta q({\rm GR}) \approx -0.009\ {\rm keV}. \qquad (103)$$

This energy redshift is 2 orders of magnitude smaller than the dominant processes that are calculated in Secs. III–VI. The dispersion in the gravitational energy shift, which would contribute to the broadening of the line, is an order of magnitude smaller, ~ 0.001 keV.

C. Collisional broadening

The effect of collisions on the coherence length for neutrino oscillations was first discussed by Nussinov [46] in a beautifully original paper(that also quantified the small probabilities for obtaining a large reduction in the electron-neutrino flux at Earth due to vacuum oscillations). Loeb [47] was the first to carry out a detailed calculation of the collisional broadening of a solar neutrino line (see also [48]). In the discussion below, I follow the treatment of Loeb.

Let $P(q)$ be the probability that a neutrino is emitted with the energy q in the presence of the solar plasma and let q_0 be the energy that would be emitted if the collisional frequency were set equal to zero. The probability distribution $P(q)$ has the usual Lorentz shape

$$P(q) = \frac{\pi^{-1}q_\tau}{(q-q_0)^2 + q_\tau^2}, \qquad (104)$$

where

$$q_\tau = (2\pi\tau)^{-1}, \qquad (105)$$

and τ is the coherence time for neutrino emission [47]. The coherence time denotes the period over which the emitting system loses its phase due to collisions with the background plasma particles.

Loeb [47] shows that the collision time for ^{7}Be ions in the solar interior is about $10^{15}\ {\rm s}^{-1}$ and that the coherence time τ is

$$\tau \approx 5\times 10^{-17}\ {\rm sec}. \qquad (106)$$

The width q_τ is therefore very small,

$$q_\tau \approx 0.013\ {\rm keV}, \qquad (107)$$

and may be neglected in the present context.

VIII. NEW PHYSICS

The two most popular mechanisms for explaining the solar neutrino problem via new physics are vacuum neutrino oscillations, first discussed in this connection by Gribov and Pontecorvo [16] in an elegant and epochal paper, and matter-enhanced neutrino oscillations, the Mikheyev-Smirnov-Wolfenstein (MSW) effect, a beautiful idea discovered by Wolfenstein [17] and by Mikheyev and Smirnov [18]. In Sec. VIII A, I present calculations of the effect of vacuum oscillations on the energy shift, Δ, of the ^{7}Be neutrino line (solar versus laboratory) and in Sec.

VIII B, I investigate the effect of matter-enhanced oscillations. Finally, in Sec. VIII C, I discuss briefly the effect of other suggested new physics processes on the energy shift. These discussions of potential (new-physics) solutions show that the physical processes considered would not be expected to change significantly the energy shift that is calculated by considering only thermal effects in the core of the Sun. The effect of the width of the ^{7}Be line on neutrino oscillations was discussed previously by Pakvasa and Pantaleone [26].

A. Vacuum oscillations

If vacuum oscillations occur, the (energy-dependent) probability that an electron-type neutrino, ν_e, that is created in the solar interior with an energy $q_{\rm obs}$ in the laboratory frame survives as an electron-type neutrino until it reaches a terrestrial detector modifies the original solar neutrino energy spectrum. Thus

$$\text{spectrum}_{\nu_e}(q_{\rm obs}) = \text{spectrum}_{\rm solar}(q_{\rm obs})\,|\langle\nu_e,\text{detect}|\nu_e,\text{emit}\rangle|^2_{q_{\rm obs}}. \tag{108}$$

If the electron-type neutrino is primarily coupled to only one other neutrino type, e.g., a muon-type neutrino, ν_μ, then the energy spectrum of the daughter neutrino is

$$\text{spectrum}_{\nu_\mu}(q_{\rm obs}) = \text{spectrum}_{\rm solar}(q_{\rm obs})\left[1 - |\langle\nu_e,\text{detect}|\nu_e,\text{emit}\rangle|^2_{q_{\rm obs}}\right]. \tag{109}$$

The probability for an electron-type neutrino to change its flavor to a muon-type neutrino can be written as [16,49,50]

$$\begin{aligned}|\langle\nu_\mu,\text{detect}|\nu_e,\text{emit}\rangle|^2_{q_{\rm obs}} &= 1 - |\langle\nu_e,\text{detect}|\nu_e,\text{emit}\rangle|^2_{q_{\rm obs}} \\ &= \sin^2 2\Theta_V \sin^2\phi(q_{\rm obs}),\end{aligned} \tag{110}$$

where Θ_V is the vacuum oscillation angle and $\phi(q_{\rm obs})$ depends upon the neutrino energy, upon the differences in the square of the masses of ν_μ and ν_e, Δm^2, the distance D between the terrestrial detector and the location in the Sun where the neutrinos are produced. Numerically,

$$\phi(q_{\rm obs}) = 1.15\times10^{11}\left(\frac{0.86\text{ MeV}}{q_{\rm obs}}\right)\left(\frac{\Delta m^2}{\text{eV}^2}\right)\left(\frac{R}{1\text{ A.U.}}\right). \tag{111}$$

As pointed out by Bahcall and Frautschi [49], the survival probability must be averaged over the neutrino energy profile in order to calculate the effect of vacuum oscillations on the observed neutrino event rates. Fine-tuning of the vacuum oscillation parameters is required to produce large effects on the observed rates. If vacuum oscillations reduce the flux of ^{8}B electron-type neutrinos (which have a broad energy profile with a total width $\sim$ 10 MeV) by a large factor (as required to explain the difference between the standard model predictions and the observations with the chlorine and Kamiokande detectors), then the mass difference squared δm^2 must cause $\phi(q_{\rm obs})$ (evaluated at $\approx$ 8 MeV) to be a small integer multiple of $\pi/2$ [49]. Thus, if vacuum oscillations are to explain the solar neutrino problem,

$$\Delta m^2(\text{big effect};^8\text{B}) \sim 10^{-10.5}\text{ eV}^2. \tag{112}$$

There have recently been several careful studies [51] of the constraints on the vacuum oscillation parameters that are implied by the existing four solar neutrino experiments [4–7]. Krastev and Petcov [51] summarize these results as

$$5\times10^{-11}\text{ eV}^2 \le \delta m^2 \le 11.1\times10^{-11}\text{ eV}^2, \tag{113}$$

$$0.75 \le \sin^2 2\Theta_V \le 1.0. \tag{114}$$

Only certain combinations of δm^2 and $\sin^2 2\Theta_V$ are allowed, but for convenience and to be conservative, I have explored the entire range in the rectangular space defined by Eqs. (113) and (114). The allowed range of $\phi(q_{\rm obs} = q_{\rm peak})$ is

$$3.5\times\pi/2 \le \phi(862.27\text{ keV}) \le 8.0\times\pi/2. \tag{115}$$

The survival probability for an electron-type neutrino does not change much over the 1 kev width of the ^{7}Be line. In order for the phase angle $\phi(q_{\rm obs})$ [defined by Eq. (111)] to change by an appreciable fraction of a radian, the observed energy must change by an amount $\Delta q_{\rm obs}$ that is much greater than the full width of the neutrino line. The line profile is not significantly affected by vacuum oscillations unless the phase angle ϕ is chosen just so as to make the electron-neutrinos at the peak of the energy ^{7}Be energy profile maximally mix into muon neutrinos, i.e., $\phi(q_{\rm peak})$ is chosen to be an odd integer multiple of $\pi/2$. Even in the case of maximum mixing, for which electron neutrinos are practically all flavor converted, the resulting muon neutrinos have essentially the same energy spectrum as the original spectrum with which the electron neutrinos are created. Therefore, the energy profile that would be detected by neutrino-electron scattering is essentially the same for maximum mixing and for no mixing. The observed rate is decreased, of course, by mixing because muon neutrinos scatter off electrons about a factor of 5 less strongly than electron neutrinos.

How can we quantify the effect of vacuum oscillations

on the ^{7}Be neutrino line profile? The most direct effect of oscillations on the ^{7}Be line profile is manifested in the difference, Δ Eq. (66), between the average energy of solar-produced neutrinos versus laboratory-produced neutrinos. Table VI presents results of numerical calculations that have been carried out by averaging the effect of vacuum oscillations over the energy profile of the ^{7}Be line that is computed using the Bahcall-Pinsonneault solar model with helium diffusion (see Sec. V A). The quantity $\Delta(\nu_e)$ that is given in Table VI is

$$\Delta(\nu_e) \equiv \frac{\int dq_{\rm obs}\text{spectrum}\,(q_{\rm obs})\left[1-\sin^2 2\Theta_V \sin^2\phi\,(q_{\rm obs})\right](q_{\rm obs}-q_{\rm lab})}{\int dq_{\rm obs}\text{spectrum}\,(q_{\rm obs})\left[1-\sin^2 2\Theta_V \sin^2\phi\,(q_{\rm obs})\right]}\,, \tag{116}$$

which is the energy shift that would be measured for electron-type neutrinos (e.g., in neutrino absorption experiments). The corresponding energy shift $\Delta(\nu_\mu)$ that would be measured with muon-type neutrinos is

$$\Delta(\nu_\mu) \equiv \frac{\int dq_{\rm obs}\text{spectrum}\,(q_{\rm obs})\sin^2\phi\,(q_{\rm obs})\,(q_{\rm obs}-q_{\rm lab})}{\int dq_{\rm obs}\text{spectrum}\,(q_{\rm obs})\sin^2\phi\,(q_{\rm obs})}\,. \tag{117}$$

TABLE VI. The effect of vacuum neutrino oscillations on the energy shift $\Delta(\nu_e)$ [see Eq. (67)], for electron neutrinos and on the energy shift $\Delta(\nu_\mu)$ for muon neutrinos is given as a function of vacuum mixing angles Θ_V and the phase-angle ϕ, see Eq. (111), evaluated at the peak of the energy spectrum at which neutrinos are created, $q_{\rm peak} = 862.27$ keV. The last column gives the energy shift Δ(e.sc.) that would be measured in an electron-scattering experiment. The survival probability, averaged over the neutrino profile, for an electron neutrino to remain an electron neutrino is given in column 3.

$\sin^2 2\Theta_V$	$2\phi(q_{\rm peak})/\pi$	Survival (ν_e)	$\Delta(\nu_e)$ (keV)	$\Delta(\nu_\mu)$ (keV)	Δ(e.sc.) (keV)
0.0	0.0	1.000	1.286	···	1.29
1.00	3.5	0.495	1.26	1.31	1.27
1.00	4.0	0.9999	1.29	···	1.29
1.00	4.5	0.507	1.32	1.26	1.31
1.0	4.6	0.352	1.33	1.26	1.31
1.0	4.7	0.212	1.35	1.27	1.31
1.0	4.8	0.100	1.39	1.27	1.31
1.0	4.9	0.027	···	1.28	1.30
1.0	5.0	0.0002	···	1.29	1.29
1.0	5.1	0.022	···	1.29	1.27
1.0	5.2	0.091	···	1.30	1.26
1.0	5.3	0.200	1.22	1.30	1.26
1.0	5.4	0.338	1.24	1.31	1.26
1.0	5.5	0.492	1.25	1.32	1.26
1.00	6.0	0.9997	1.29	···	1.29
1.00	7.0	0.0004	···	1.29	1.29
1.0	7.2	0.089	···	1.300	1.25
1.0	7.4	0.335	1.22	1.32	1.25
1.0	7.6	0.643	1.25	1.36	1.26
1.0	7.8	0.897	1.27	1.45	1.27
1.0	8.0	0.9995	1.28	···	1.28
0.75	3.5	0.621	1.27	1.31	1.28
0.75	4.0	0.9999	1.29	···	1.29
0.75	4.5	0.630	1.30	1.26	1.30
0.75	5.0	0.250	1.29	1.29	1.29
0.75	6.0	0.9998	1.29	···	1.29
0.75	7.0	0.250	1.29	1.28	1.29
0.75	8.0	0.9996	1.29	···	1.29

For neutrino-electron scattering experiments, the energy shift that would be measured, $\langle\Delta\rangle_{\text{el sc}}$, is

$$\langle\Delta\rangle_{\text{el sc}} \equiv \frac{\sigma_e \text{survival}\,(\nu_e)\,\Delta_e + \sigma_\mu\,[1 - \text{survival}\,(\nu_e)]\,\Delta_\mu}{\sigma_e \text{survival}\,(\nu_e) + \sigma_\mu\,[1 - \text{survival}\,(\nu_e)]} \,. \tag{118}$$

I list in Table VI representative numerical results obtained for the two extreme values of the vacuum mixing angle: $\sin^2 2\Theta_V = 1.00$ and $\sin^2 2\Theta_V = 0.75$ [cf. Eq. (114)]; intermediate choices of the vacuum mixing angle yield intermediate effects that can be approximately interpolated from Table VI. I do not list values when the component in question carries less than 10% of the flux, since these cases are not relevant for currently feasible experiments.

The numerical calculations show that the energy shift Δ for both electron and muon neutrinos is within 10% of the shift, 1.29 keV, calculated in the absence of vacuum oscillations for all cases in which the corresponding neutrino flux (electron or muon) is not less than 10% of the total flux. A change of a given sign in the energy shift for electron neutrinos, $\Delta(\nu_e)$, implies a change of the opposite sign in the energy shift for muon neutrinos, $\Delta(\nu_\mu)$. The calculated energy shift $\langle\Delta\rangle_{\text{el sc}}$, which should be used in making comparisons with electron-neutrino scattering experiments, is always within 3% of the no-oscillation value of 1.29 keV.

B. An MSW solution

The MSW solution, matter-induced neutrino oscillations, to the solar neutrino problem has been discussed by many authors [17,18,22]. For matter-enhanced oscillations, the probability of neutrino mixing within the Sun depends upon neutrino energy, but not in as delicate a fashion as for vacuum oscillations. The dependence of the survival probability on energy can be represented as a smooth function of energy over the extent of the ^{7}Be line profile [13,17,18,22]. The dimensionless ratio that determines the amount by which the MSW effect changes the line profile is the ratio of the neutrino line width to the characteristic energy of the line. This ratio is very small: $\text{FWHM}/2q_{\text{peak}} = 0.1\%$.

Large suppressions of electron-type neutrinos are achieved by the MSW effect without fine-tuning with respect to the neutrino energy. In fact, it does not seem possible to fine-tune MSW solutions to an accuracy that would greatly amplify the small dimensionless ratio of FWHM to q_{peak} and thereby affect significantly the line profile of a large fraction of the ^{7}Be solar neutrino flux. In the resonance condition, the neutrino energy, q_{res}, is inversely proportional to the electron density n_e at the resonance position [13,17,18]. The change in the electron density over the region of production of ^{7}Be neutrinos is [13] $\Delta n_e/n_e \approx 0.25$, while the change in neutrino energy over the line profile is $\Delta q/q < 0.001$. If one tried to invent a situation in which only part of the ^{7}Be line profile went through resonance, the fine-tuning that applied at one location would quickly be destroyed as the electron density changed by a tiny amount (and therefore changed the resonance condition) within the region in which the neutrinos are produced.

C. Some other new physics processes

Other solutions have been proposed for the solar neutrino problem that involve new weak interaction physics. These other solutions include rotation of the neutrino magnetic moment [20], matter-enhanced magnetic moment transitions [21], and neutrino decay [52]. The classical magnetic moment transition is independent of energy and does not affect the shape of the line profile. Matter-enhanced magnetic-moment transitions, such as MSW transitions, are not fine-tuned, vary smoothly with energy, and depend upon a resonant electron density that varies from point to point. Therefore, the argument given above for the MSW effect also applies to matter-enhanced magnetic-moment transitions. Neutrino decay involves characteristic energies that are very large compared to the total width of the ^{7}Be line and is also not fine-tuned. Hence, none of these processes would change significantly the shape of the ^{7}Be line profile.

IX. THE ^{7}LI NEUTRINO ABSORPTION CROSS SECTION

The calculated absorption cross section for the reaction

$$\nu_e + {}^7\text{Li} \rightarrow {}^7\text{Be} + e^-, \quad E_{\text{th}} = 861.9 \text{ keV}, \tag{119}$$

where ν_e is produced by ^{7}Be electron capture in the Sun, depends upon the assumed energy profile of the solar neutrinos [37,38]. Neutrinos with energies below the energy threshold, E_{th}, for the laboratory reaction, Eq. (119), cannot be absorbed. The energy threshold of 861.90 keV [cf. Eq. (6)] falls within the line profile shown in Fig. 2. The precise location of the threshold within the line profile determines the fraction of emitted neutrinos that can be absorbed by ^{7}Li.

The average absorption cross section for solar-produced ^{7}Be neutrinos incident on a laboratory detector of ^{7}Li is

$$\langle \text{spectrum}_{\nu_e}(q_{\text{obs}})\,\sigma_{\text{abs}}(q_{\text{obs}})\rangle \simeq 19 \times 10^{-46} \text{ cm}^2, \tag{120}$$

assuming neutrinos do not change flavor after their creation. To the accuracy shown, the results are identical for ^{7}Be line profiles calculated using the standard models [15] with and without helium diffusion (cf. rows 1 and 2 of Table III). As usual, Eq. (120) includes a correction to take account of the fact that only 89.7% of the ^{7}Be neutrinos are produced in ground-state to ground-state transitions.

The cross section given in Eq. (120) is almost a factor of 2 larger than obtained previously [37,38], which should make the contemplated radiochemical experiments somewhat easier than originally considered [30]. The earlier

treatments neglected the difference in electron binding energies of solar and laboratory ^{7}Be atoms as well as Doppler shifts of the ^{7}Be nuclei, and did not average over the temperature profile of the sun. In the present calculation, 88% of the ^{7}Be neutrinos are above threshold for the reaction Eq. (119). For the earlier calculation [38], only about 50% were above threshold. The difference between a cumulative probability of 50% and a cumulative probability of 88% corresponds to an average energy shift of 0.85 keV for the line profile shown in Fig. 2.

X. SUMMARY

The temperature distribution of the solar core is expressed robustly in the neutrino energy profile that results from ^{7}Be electron capture. The characteristics of the line profile, shown in detail in Figs. 2 and 3, are independent of uncertain details regarding solar models and instead reflect the global thermal properties of the solar interior. The robustness of the computed characteristics of the ^{7}Be line profile derives from the well-determined thermal structure of the solar-model description of the interior of the Sun (cf. Sec. V A). For the most precise standard solar models computed over the past decade, 1982–1992, and listed in Table III, the central temperature has varied over a total range of $\pm 0.5\%$, $T_c = (15.58 \pm 0.08) \times 10^6$ K. The ^{7}Be and the ^{8}B neutrino fluxes have varied by $\pm 6\%$. The relative number of electron captures that occur from bound orbits is 0.221 ± 0.006 for all the solar models of Table III. For a heterogeneous set of ten recently calculated solar models, listed in Table IV, that were generally not required to have the highest attainable precision, the central temperature varied by $\pm 1\%$, $T_c = (15.55 \pm 0.15) \times 10^6$ K.

The following paragraphs summarize the principal results obtained in this paper. In addition, Tables II and III present numerical representations of the line profiles and Table V provides a concise summary of the potentially measurable characteristics that were calculated using different solar models. The numerical values for the energy shift Δ and the low-energy and high-energy half-widths of the line profile are calculated in Sec. V.

The shift in average neutrino energy Δ between ^{7}Be neutrinos emitted in the Sun and ^{7}Be neutrinos produced in the laboratory is $\Delta(\text{g.s.}) = 1.29$ keV for ground-state captures and the physical parameters of the most accurate available solar model (which includes helium diffusion). Calculations with other models yield values of the energy shift for ground-state decays of 1.28 keV, 1.28 keV, and 1.23 keV (for a 1982 solar model with only 19 shells in the region in which ^{7}Be neutrinos are produced). The shift for excited-state decays is $\Delta(\text{e.s.}) = 1.24$ keV. These calculated energy shifts take account of the fact that approximately 88% of the captures involve electrons in continuum orbits and only about 22% involve electrons that are bound to the decaying nucleus. The atomic binding energies that are released when ^{7}Be nuclei capture electrons in the Sun (or in the laboratory) are evaluated in Sec. II.

The low-energy half-width, W_-, of the line profile is (0.55 ± 0.02) keV for the ground-state decay (0.24 keV for the excited-state decay, see column 5 of Table V). Here W_- is the half-width of the energy profile below the peak in the probability distribution. This low-energy part of the line is primarily determined by Doppler shifts caused by the thermal velocities of ^{7}Be ions that are moving away from the detector located on Earth. The low-energy side of the profile is approximately Gaussian in shape, reflecting the Doppler origin of this part of the energy spectrum.

The high-energy half-width W_+ of the line profile is 1.07 keV for the ground-state decay (0.73 keV for the excited-state decay, see column 6 of Table V) and is determined primarily by the center-of-momentum kinetic energies of the electrons and the ^{7}Be nuclei that take part in electron capture reactions. The high-energy side of the line profile is approximately exponential in shape, with a probability distribution that is proportional to $\exp(-q_{\text{obs}}/T_{\text{eff}})$ where q_{obs} is the neutrino energy that is observed in the laboratory and $T_{\text{eff}} \approx 1.31$ keV (15.1×10^6 K). The exponential side of the probability distribution results from an average (in the solar model) over the different exponential distributions of center-of-momentum energies (electrons and ions) that apply at each solar radius.

The principal characteristics of the line profile are derived by approximate analytic calculations in Sec. VI, calculations that elucidate the physical origins of the various effects. The most remarkable result obtained in Sec. VI is that the energy shift, Δ, is essentially identical for the ground-state and the excited-state captures (cf. Fig. 1). The average shift is shown in Sec. VI to be independent of the typical emitted neutrino energy (384 keV or 862 keV) because the rest-mass energy of a ^{7}Be nucleus is much larger than the solar thermal energies (see discussion in Sec. VI B).

The energy shift is, to a good approximation, equal to the average temperature of the solar interior weighted by the fraction of ^{7}Be neutrinos that are produced at each temperature, i.e., $\int_\odot dT T d\phi(^7\text{Be}, T) / \int_\odot dT d\phi(^7\text{Be}, T)$, where $d\phi(^7\text{Be}, T)$ is the flux of ^{7}Be neutrinos produced at the local temperature T [cf. Eq. (92)]. The ^{7}Be neutrinos are produced in the inner few percent of the solar mass [13], essentially all in the region $(0.04 \pm 0.03)\, M_\odot$. Therefore, a measurement of the energy shift is a measurement of the central temperature distribution of the Sun.

The most striking aspect of the computed energy profile is the asymmetry between the Gaussian low-energy side and the exponential high-energy side (cf. Figs. 2 and 3). Doppler shifts caused by the thermal velocities of the ^{7}Be nuclei produce a symmetric, Gaussian contribution to the line broadening, which determines the shape of the energy profile at energies below the peak. The higher-energy part of the profile is determined by the center-of-momentum kinetic energies. The exponential distribution of kinetic energies produces an exponential tail for large neutrino energies. The positive-definite character of the kinetic energies is responsible for the asymmetry.

Electrostatic screening, particle collisions, and gravita-

tional redshifts all contribute to the line broadening, but their effects are much smaller than the effect caused by thermal broadening (Sec. VII).

Vacuum neutrino oscillations can be fine-tuned to produce maximal mixing of neutrino flavors near the peak of the ^{7}Be neutrino line. But, the energy shift of the dominant neutrino survivor is always close to the unmixed value of $\Delta = 1.29$ keV (see Table VI). The invariance of the line shape results from the fact that the oscillation phase changes significantly only over an energy range that is much larger than the line shape (see Sec. VIII A).

The energy profile of the ^{7}Be neutrino line should be taken into account (using Tables II and III) in precise calculations of what is to be expected from vacuum neutrino oscillations. It has become standard in calculations of the effects of vacuum oscillations to take account of the variation of the distance between the point of creation of the neutrinos and the point of detection. The variation in the point of creation corresponds to a phase change of order 10^{-4}, since the ratio of the solar radius to the Earth-Sun distance is about 0.005 and the ^{7}Be neutrinos are produced in a region of about $\pm 0.025 R_\odot$. On the other hand, the width of the ^{7}Be line profile is about 10^{-3} of the average ^{7}Be neutrino energy. Therefore, the change in phase due to the energy width of the neutrino line is about an order of magnitude larger than the phase change caused by averaging over the region of production.

The MSW solutions that are consistent with existing solar neutrino experiments vary smoothly with energy and are not fine-tuned. The variation of the resonant electron density within the Sun prevents fine-tuning of the solution over a small energy range such as the width of the ^{7}Be neutrino line. For MSW solutions, the fractional change in the electron-type neutrino survivability over the energy profile of the ^{7}Be line is small. Other solutions of the solar neutrino problem that involve new physics like rotation of the neutrino magnetic moment, matter-enhanced magnetic-moment transitions, and neutrino decay are also not expected to change significantly the shape of the ^{7}Be line profile.

The energy shift and the shape of the ^{7}Be neutrino energy profile affect significantly the computed value of the absorption cross section for ^{7}Be solar neutrinos incident on a ^{7}Li detector (see Sec. IX).

ACKNOWLEDGMENTS

This work was supported by NSF Grant No. PHY92-45317. I am grateful to B. Cabrera, F. Calaprice, E. Fiorini, M. Giammarchi, A. Gould, M. Kamionkowski, M. Lowry, P. Krastev, R. Kulsrud, A. Loeb, M. N. Rosenbluth, M. Schwarzschild, A. Y. Smirnov, E. Witten, and T. Ypsilantis for valuable discussions and suggestions.

[1] J. N. Bahcall, Phys. Rev. Lett. **12**, 300 (1964); R. Davis, Jr., *ibid.* **12**, 302 (1964).

[2] R. Davis, Jr., D. S. Harmer, and K. C. Hoffman, Phys. Rev. Lett. **20**, 1205 (1988).

[3] J. N. Bahcall and R. Davis, Jr., Science **191**, 264 (1976).

[4] R. Davis, Jr., in *Neutrino '88*, Proceedings of Thirteenth Conference on Neutrino Physics and Astrophysics, Boston, Massachusetts, 1988, edited by J. Schneps *et al.* (World Scientific, Singapore, 1989), p. 518.

[5] K. S. Hirata *et al.*, Phys. Rev. D **44**, 2241 (1991).

[6] P. Anselmann *et al.*, Phys. Lett. B **285**, 376 (1992).

[7] A. I. Abazov *et al.*, Phys. Rev. Lett. **67**, 3332 (1991).

[8] G. Aardsma *et al.*, Phys. Lett. B **194**, 321 (1987); G. Ewan *et al.*, Sudbury Neutrino Observatory Proposal SNO-87-12 (1987); H. Chen, Phys. Rev. Lett. **55**, 1534 (1985).

[9] Y. Totsuka, in *Proceedings of the International Symposium on Underground Physics Experiments*, edited by K. Nakamura (ICRR, University of Tokyo, 1990), p. 129; A. Suzuki, in *Proceedings of the Workshop on Elementary-Particle Picture of the Universe*, Tsukuba, Japan, 1987, edited by M. Yoshimura, Y. Totsuka, and K. Nakamura (KEK Report No. 87-1, Tsukuba, 1987), p. 136.

[10] R. S. Raghavan, in *Proceedings of the XXVth International Conference on High Energy Physics*, Singapore, 1990, edited by K. K. Phua and Y. Yamaguchi (World Scientific, Singapore, 1990), Vol. 1, p. 482; G. Ranucci for the Borexino Collaboration, Nucl. Phys. B (Proc. Suppl.) 32, 149 (1993); C. Arpasella *et al.*, in "Borexino at Gran Sasso: Proposal for a real-time detector for low energy solar neutrinos," Vols. I and II, University of Milan, INFN report (unpublished).

[11] J. N. Bahcall, M. Baldo-Ceolin, D. Cline, and C. Rubbia, Phys. Lett. B **178**, 324 (1986); ICARUS Collaboration, ICARUS I: "An optimized, real-time detector of solar neutrinos," Frascati Report No. LNF-89/005 (R), 1989 (unpublished); C. Rubbia, CERN-EP Internal Report No. 77-8, 1977 (unpublished).

[12] J. N. Bahcall and H. A. Bethe, Phys. Rev. Lett. **65**, 2233 (1990); Phys. Rev. D. **47**, 1298 (1993).

[13] J. N. Bahcall, *Neutrino Astrophysics* (Cambridge University Press, Cambridge, England, 1989).

[14] J. N. Bahcall and R. K. Ulrich, Rev. Mod. Phys. **60**, 297 (1988).

[15] J. N. Bahcall and M. H. Pinsonneault, Rev. Mod. Phys. **64**, 885 (1992).

[16] V. Gribov and B. Pontecorvo, Phys. Lett. **28B**, 493 (1969); S. M. Bilenky and B. Pontecorvo, Phys. Rep. **41**, 225 (1978); S. M. Bilenky and S. T. Petcov, Rev. Mod. Phys. **59**, 671 (1987); see also B. Pontecorvo, Zh. Eksp. Teor. Fiz. **53**, 1717 (1967) [Sov. Phys. JETP **26**, 984 (1968)].

[17] L. Wolfenstein, Phys. Rev. D **17**, 2369 (1978); **20**, 2634 (1979).

[18] S. P. Mikheyev and A. Yu. Smirnov, Yad. Fiz. **42**, 1441 (1985) [Sov. J. Nucl. Phys. **42**, 913 (1985)]; Zh. Eksp. Teor. Fiz. **91**, 7 (1986) [Sov. Phys. JETP **64**, 4 (1986)]; Nuovo Cimento **9C**, 17 (1986); T. K. Kuo and J. Panta-

leone, Rev. Mod. Phys. **61**, 937 (1989); S. P. Mikheyev and A. Yu. Smirnov, Progr. Part. Nucl. Physics **23**, 41 (1989).

[19] E. Roulet, Phys. Rev. D **44**, R935 (1991); M. M. Guzzo, A. Masiero, and S. T. Petcov, Phys. Lett. B **260**, 154 (1991); V. Barger, R. J. N. Phillips, and K. Whisnant, Phys. Rev. D. **44**, 1629 (1991); see also, J. W. F. Valle, Phys. Lett. B **199**, 432 (1987).

[20] A. Cisneros, Astrophys. Space Sci. **10**, 87 (1971); J. Schechter and J. W. F. Valle, Phys. Rev. D **24**, 1883 (1981); M. B. Voloshin, M. I. Vysotsky, and L. B. Okun, Zh. Eksp. Teor. Fiz. **91**, 754 (1986) [Sov. Phys. JETP **64**, 446 (1986)]; M. B. Voloshin and M. I. Vysotsky, Yad. Fiz. **44**, 845 (1986) [Sov. J. Nucl. Phys. **44**, 544 (1986)]; L. B. Okun, *ibid.* **44**, 847 (1986) [**44**, 546 (1986)].

[21] C. S. Lim and W. J. Marciano, Phys. Rev. D **37**, 1368 (1988); E. Kh. Akhmedov, Phys. Lett. B **213**, 64 (1988).

[22] P. B. Pal, Int. J. Mod. Phys. A **7**, 5387 (1992); S. M. Bludman, N. Hata, D. C. Kennedy, and P. G. Langacker, Phys. Rev. D **47**, 2220 (1993).

[23] J. N. Bahcall, Phys. Rev. **128**, 1297 (1962); A. G. W. Cameron, Annu. Rev. Nucl. Sci. **8**, 299 (1958).

[24] I. Iben, K. Kalata, and J. Schwartz, Astrophys. J. **150**, 1001 (1967).

[25] J. N. Bahcall, Phys. Rev. Lett. **71**, 2369 (1993).

[26] S. Pakvasa and J. Pantaleone, Phys. Rev. Lett. **65**, 2479 (1990); J. Pantaleone, Phys. Rev. D **43**, 2346 (1991).

[27] *Table of Isotopes*, edited by C. M. Lederer and V. S. Shirley (Wiley, New York, 1978), p. 3; F. Ajzenberg-Selove, Nucl. Phys. A **490**, 1 (1988).

[28] J. N. Bahcall, Phys. Rev. D **44**, 1644 (1991).

[29] A. Drukier and L. Stodolsky, Phys. Rev. D **30**, 2295 (1984); B. Cabrera, L. M. Krauss, and F. Wilczek, Phys. Rev. Lett. **55**, 25 (1985); R. E. Lanou, H. J. Maris, and G. M. Seidel, *ibid.* **58**, 2498 (1987); *Low Temperature Detectors for Neutrinos and Dark Matter*, Proceedings of the Workshop, Tegernsee, West Germany, 1987, edited by K. Pretzl, N. Schmitz, and L. Stodolsky (Springer, New York, 1987); G. Laurenti *et al.*, in *Neutrino Telescopes 1993*, edited by M. Baldo-Ceolin (Papergraf, Padova)(to be published).

[30] J. K. Rowley, in *Proceedings of the Informal Conference on the Status and Future of Solar Neutrino Research*, edited by G. Friedlander (Brookhaven National Laboratory, Upton, New York, 1978), Report No. 50879, p. 265; G. S. Hurst *et al.*, Rev. Mod. Phys. **51**, 767 (1979); E. P. Veretenkin, V. N. Gavrin, and E. A. Yanovich, Sov. J. At. En. **55**, 82 (1985); T. Litherland, E. L. Fireman, and J. K. Rowley, Nucl. Instrum. Methods **B29**, 387 (1987); W. C. Haxton, Phys. Rev. Lett. **60**, 768 (1988); S. N. Danshin *et al.*, report, Institute for Nuclear Research of RAS, Moscow, 1993, in *Proceedings of International Symposium on Neutrino Telescopes*, Venice, edited by M. Baldo-Ceolin (to be published).

[31] R. S. Raghavan, P. Raghavan, and T. Kovacs, AT&T Bell Laboratories Technical Memorandum 11121-930824-27TM, 1993 (unpublished).

[32] D. O. Caldwell *et al.*, Phys. Rev. Lett. **61**, 510 (1988); B. A. Young *et al.*, *ibid.* **64**, 2795 (1990); E. Fiorini, Physica B **167**, 388 (1991); A. Alessandrello *et al.*, Nucl. Phys. **B31**, 83 (1993); R. L. Mossbauer, in *Weak Interactions and Neutrinos*, Proceedings of the Workshop, Ginosar, Israel, 1989, edited by P. Singer and B. Gad Rilam [Nucl. Phys. B (Proc. Suppl.) **13**, 385 (1993)]; E. Fiorini, Physica B **167**, 388 (1991); D. McCammon, M. Juda, J. Zhang, S. Holt, R. Kelley, S. H. Moseley, and A. Szymkowiak, Jpn. J. Appl. Phys. **26**, 2084 (1987).

[33] A. Alessandrello *et al.*, Report No. INFN/SAE-92/28, "A Cryogenic Experiment for Solar Neutrino Spectroscopy and Search for Dark Matter," 11 November 1992 (unpublished); E. Fiorini, in *Proceedings of International Symposium on Neutrino Telescopes* [30].

[34] J. Seguinot, T. Ypsilantis, and A. Zichini, "A High Rate Solar Neutrino Detector with Energy Determination," Report No. LPC92-31, College de France, 12/8/92 (unpublished); C. Laurenti, S. Tzamarias, G. Bonvicini, A. Zichichi, J. Sequinot, and T. Ypsilantis, Report No. CERN/LAA/PC193-10 (unpublished).

[35] J. N. Bahcall and C. P. Moeller, Astrophys. J. **155**, 511 (1969).

[36] W. Watson and E. E. Salpeter, Astrophys. J. **181**, 237 (1973).

[37] G. V. Domogatsky, Lebedev Phys. Inst. Report No. 153, 1969 (unpublished).

[38] J. N. Bahcall, Rev. Mod. Phys. **50**, 881 (esp. Sec. IV) (1978).

[39] C. W. Johnson, E. Kolbe, S. E. Koonin, and K. Langanke, Astrophys. J. **392**, 320 (1992).

[40] *Handbook of Chemistry and Physics*, edited by R. C. Weast and M. J. Astle (CRC Press Inc., Boca Raton, Florida, 1979), p. E68.

[41] E. J. Konopinski, *Theory of Beta Radioactivity* (Oxford University Press, Oxford, 1966); E. C. Commins, *Weak Interactions* (McGraw-Hill, New York, 1973); B. R. Holstein, *Weak Interactions in Nuclei* (Princeton University Press, Princeton, 1989).

[42] E. J. Konopinski, Annu. Rev. Nuclear Sci. **9**, 99 (1959).

[43] J. N. Bahcall, Astrophys. J. **139**, 318 (1964).

[44] J. N. Bahcall, W. F. Huebner, S. H. Lubow, P. D. Parker, and R. K. Ulrich, Rev. Mod. Phys. **54**, 767 (1982).

[45] Y. Lebreton and W. Däppen, in *Seismology of the Sun and Sun-like Stars*, edited by V. Domingo and E. J. Rolfe (ESA SP-286, 1988), p. 661; I. J. Sackmann, A. I. Boothroyd, and W. A. Fowler, Astrophys. J. **360**, 727 (1990); C. R. Proffitt and G. Michaud, Astrophys. J. **380**, 238 (1991); J. A. Guzik and A. N. Cox, Astrophys. J. Lett. **381**, 333 (1991); B. Ahrens, M. Stix, and M. Thorn, Astron. Astrophys. **264**, 673 (1992); J. Christensen-Dalsgaard, Geophys. Astrophys. Fluid Dynamics **62**, 123 (1992); D. B. Guenther, P. Demarque, Y. C. Kim, and M. H. Pinsonneault, Astrophys. J. **387**, 372 (1992); G. Berthomieu, J. Provost, P. Morel, and Y. Lebreton, Astron. Astrophys. **268**, 775 (1993); S. Turck-Chièze and I. Lopes, Astrophys. J. **408**, 347 (1993); V. Castellani, S. Degl'Innocenti, and G. Fiorentini, Astron. Astrophys. **271**, 601 (1993).

[46] S. Nussinov, Phys. Lett. **63B**, 201 (1976).

[47] A. Loeb, Phys. Rev. D **39**, 1009 (1989).

[48] L. Krauss and F. Wilczek, Phys. Rev. Lett. **55**, 122 (1985).

[49] J. N. Bahcall and S. C. Frautschi, Phys. Lett. B **29**, 623 (1969).

[50] S. M. Bilenky and B. Pontecorvo, Phys. Rev. D **41**, 225 (1978); V. Barger, R. J. N. Phillips, and K. Whisnant, *ibid.* **24**, 538 (1981); S. L. Glashow and L. M. Krauss, Phys. Lett. B **190**, 199 (1987).

[51] P. I. Krastev and S. T. Petcov, Phys. Lett. B **299**, 99 (1993); **288**, 85 (1992); V. Barger, R. J. N. Phillips, and

K. Whisnant, Phys. Rev. Lett. **69**, 3135 (1992); A. Acker, S. Pakvasa, and J. Pantaleone, Phys. Rev. D **43**, R1754 (1991); V. Barger, R. J. N. Phillips, and K. Whisnant, *ibid.* **43**, 1110 (1991).

[52] J. N. Bahcall, N. Cabibbo, and A. Yahil, Phys. Rev. Lett. **28**, 316 (1972); S. Pakvasa and K. Tennakone, *ibid.* **28**, 1415 (1972); Z. G. Berezhiani and M. I. Vysotsky, Phys. Lett. B **199**, 281 (1987); J. Frieman, H. Haber, and K. Freese, *ibid.* **200**, 115 (1988); X.-G. He, S. Pakvasa, and R. S. Raghavan, Phys. Rev. D **38**, 1317 (1988); A. Acker, A. Joshipura, and S. Pakvasa, Phys. Lett. B **285**, 371 (1992); Z. G. Berezhiani, G. Fiorentini, M. Moretti, and A. Rossi, Z. Phys. C **54**, 581 (1992).